AD-A034 020 AIRESEARCH MFG CO OF ARIZONA PHOENIX F/G 20/4
A NUMERICAL METHOD FOR HIGH REYNOLDS NUMBER VISCOUS SEPARATED F--ETC(U)
SEP 76 P R DODGE, L S LIEBER N00014-74-C-0317
UNCLASSIFIED 74-211196(6) NL

1 OF 1
AD A034020

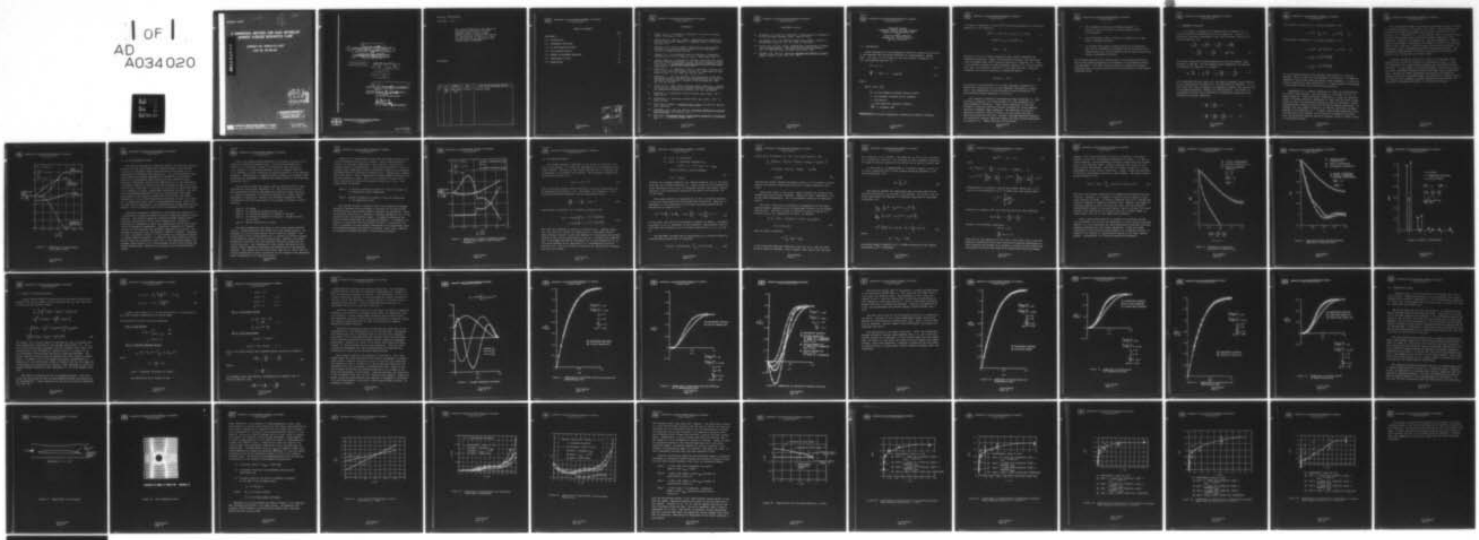

END

DATE FILMED
2-77

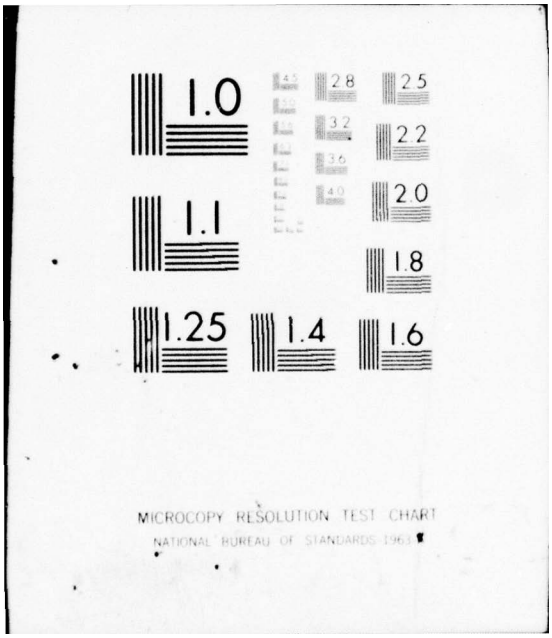
1.0
1.1
1.25
1.4
1.6
1.8
2.0
2.2
2.5
2.8
3.2
3.6
4.0
MICROCOPY RESOLUTION TEST CHART
NATIONAL BUREAU OF STANDARDS 1963

TECHNICAL REPORT

A NUMERICAL METHOD FOR HIGH REYNOLDS NUMBER VISCOUS SEPARATED FLOW

CONTRACT NO. N00014-74-C-0317

TASK NO. NR 061-221

AIRESEARCH MANUFACTURING COMPANY OF ARIZONA
A DIVISION OF THE GARRETT CORPORATION
402 South 36th Street, Phoenix, Arizona 85034

74-211196(6)
Sept. 30, 1976

(9) TECHNICAL REPORT

(6) A NUMERICAL METHOD FOR HIGH REYNOLDS NUMBER VISCOUS SEPARATED FLOW

FOR

(15) OFFICE OF NAVAL RESEARCH
CONTRACT NO. N00014-74-C-0317
TASK NO. NR 061-221

(14) 74-211196(6)

September 30, 1976

(11) 30 Sep 76

(12) 55 p.

(10) Prepared by Paul R. Dodge and L. S. Lieber

Initial Issue Approved by Dale R Dodge

P. R. Dodge,
Principal Investigator

D. G. Culy

D. G. Culy, Program Manager

AIRESEARCH MANUFACTURING COMPANY
A DIVISION OF THE GARRETT CORPORATION
PHOENIX, ARIZONA

404796

REPORT NO. 74-211196(6)

TOTAL PAGES 52

This data presented in this report is sponsored by the Office of Naval Research under Contract Number N00014-74-C-0317, Task No. NR 061-221, and reproduction in whole or in part is permitted for any purpose of the United States Government.

ATTACHMENTS:

REV	BY	APPROVED	DATE	PAGES AND/OR PARAGRAPHS AFFECTED
NC	HBJ/ FMB	See Title Page	9-30-76	Initial Issue

TABLE OF CONTENTS

AIRESEARCH MANUFACTURING COMPANY OF ARIZONA
A DIVISION OF THE GARRETT CORPORATION
PHOENIX, ARIZONA

REFERENCES

1. Dodge, Paul R., "A Numerical Method for 2-D and 3-D Viscous Flows", AIAA paper 76-425.

2. Dodge, Paul R., and L.S. Lieber, "Separated Flow Program for the Office of Naval Research", AiResearch Report 74-211196(5), February 1976.

3. Warming, R.F., and B.J. Hyett, "The Stability and Accuracy Analysis of Finite-Difference Method", to be published in Journal of Computational Physics.

4. Pratap, V.S., A.K. Majumdar, and D.B. Spalding, "Numerical Computation of Flow in Rotating Ducts", ASME paper 76-FE-25.

5. Carter, James E., and Stephen F. Wornom, "Solutions for Incompressible Separated Boundary Layers Including Viscous-Inviscid Interaction, in Aerodynamic Analysis Requiring Advanced Computers, Part I, NASA SP-347, March 1975.

6. Catherall, D., K. Stewartson, and P.G. Williams, "Viscous Flow Past a Flat Plate with Uniform Injection", Proceedings of the Royal Society, A, Vol. 284, pp 370-395, 1965.

7. Catherall, D., and K.W. Mangler, "The Integration of Two Two-Dimensional Laminar Boundary-Layer Equations Past the Point of Vanishing Skin Friction", Journal of Fluid Mechanics, 1966, Vol. 26, pp 163-182.

8. Leigh, D.C.F., "The Laminar Boundary Layer Equations: A Method of Solution by Means of an Automatic Computer", proceedings of the Cambridge Philosophical Society, Vol. 51, pp-320-322.

9. Goldstein, S., Quarterly Journal of Mech. Appl. Math., Vol. 1 1948, pp 43.

10. Stewartson, K., Quarterly Journal Mech. Appl. Math., Vol. II 1958, pp 399.

11. Schlichting, Hermann, Boundary-Layer Theory 6th Edition, McGraw-Hill, New York.

12. Richtmyer, R.D., and K.W. Morton, Difference Methods for Initial Value Problems, 2nd Edition, 1967.

13. Ames, W.F., Nonlinear Partial Differential Equations in Engineering, Vol. II, Academic Press, 1972.

REFERENCES (Contd)

14. Schubauer, G.B. and P.S. Klebanoff, "Investigation of Separation of the Turbulent Boundary Layer", NACA TN 1030.

15. van Driest, E.R., "On Turbulent Flow Near a Wall", Journal of Aeronautical Science, Vol. 23, 1956, pp 1007-1011.

16. Coles, D.E. and E.A. Hirst, "Proceedings, Computation of Turbulent Boundary Layers - 1968 AFOSR-IFP-Standard Conference", Vol. II, Compiled Data, Stanford University, 1969.

17. Launder, B.E. and D.B. Spalding, Mathematical Models of Turbulence, Academic Press, New York, 1972.

AIRESEARCH MANUFACTURING COMPANY OF ARIZONA
A DIVISION OF THE GARRETT CORPORATION
PHOENIX, ARIZONA

TECHNICAL REPORT
A NUMERICAL METHOD FOR HIGH REYNOLDS
NUMBER VISCOUS SEPARATED FLOW
FOR
OFFICE OF NAVAL RESEARCH
CONTRACT NO. N00014-74-C-0317
TASK NO. NR 061-221

1.0 INTRODUCTION

Dodge (Reference 1**) has presented a method for numerical solutions to the momentum and continuity equations of incompressible, steady flow. The heart of this method is the substitution of Equation (1) into the momentum Equation (2):

$$\vec{W} = \nabla\phi + \vec{u} \tag{1}$$

$$\frac{D\vec{W}}{Dt} = -\nabla P/\rho + \nabla \cdot \nu_e(\text{def } \vec{W}) \tag{2}$$

where:

$$\text{def } \vec{W} = \nabla\vec{W} + (\nabla\vec{W})^*$$

$\vec{W}$ = is the ensemble averaged velocity vector

P = the ensemble averaged static pressure

ρ = the density

ν_e = the effective kinematic viscosity

$(\nabla\vec{W})^*$ = transpose $(\nabla\vec{W})$

**References are located immediately following the Table of Contents

The result is Equation (3) for $\vec{u}$ and, with the application of continuity, Equation (4) for potential.

$$(\vec{W}\cdot\nabla)\ \vec{u} + (\vec{u}\cdot\nabla)\ \nabla\phi = \nu_e \nabla^2 \vec{u} + \nu_e\ \nabla\ (\nabla^2\phi) \qquad (3)$$

$$+ (\text{def}\ \vec{u})\ \nabla\nu_e + 2\ \left|\nabla(\nabla\phi)\right|^*\ \nabla\nu_e$$

$$\nabla^2\phi = -\nabla\cdot\vec{u} \qquad (4)$$

Equation (4) is, of course, elliptical and a direct candidate for relaxation solutions. During the relaxation solution, the right-hand side is assumed known from a previous solution to Equation (3). Since $\nabla\phi$ is directly related to static pressure, Equation (5), one can anticipate that its variation, unlike $\vec{W}$, is slow near the wall. Thus the relaxation grid can be relatively uniform and sparse.

$$(\nabla\phi\cdot\nabla)\nabla\phi = -\nabla P/\rho \qquad (5)$$

The result is the relaxation of a single dependent variable on a sparse grid instead of four or more dependent variables on a dense grid. The disadvantage is the necessity of solving Equation (3), and iterating between Equations (3) and (4).

The iteration process is discussed by Dodge (Reference 1). The solution to Equation (3) would be easy if it were parabolic in a quasi-streamline direction. Under these conditions it could be solved by a one-pass marching solution analogous to those commonly applied to boundary layer equations. The advantage of such an approach is obvious, since a solution is very rapid even when a dense grid system is utilized. However, although marching solutions are attractive, several obstacles remain for their direct application to Equation (3). Among these are the following:

- The streamwise diffusion term makes Equation (3) elliptic, and thus creates a non-well-posed initial value problem.

- At the separation point, there is a possibility of some form of singular behavior.

- In the back flow region, beyond the point of separation, the flow of information is against the marching direction, which results in a non-well-posed initial value problem even without streamwise diffusion.

The following sections will discuss each of the above difficulties with an eye toward preserving the structure of the numerical method outlined above. The final section presents a comparison between a separated-flow calculation and data as an illustration of the methods discussed below.

2.0 STREAMWISE DIFFUSION

It is useful to examine the simpler forms of Equation (3) to discover pertinent characteristics of this equation. Equation (3), written in Cartesian coordinates x and y with constant viscosity, is given by Equation (6):

$$W_x \frac{\partial u_x}{\partial x} + W_y \frac{\partial u_x}{\partial y} + u_x \frac{\partial^2 \phi}{\partial x^2} + u_y \frac{\partial^2 \phi}{\partial x \partial y}$$

$$= \nu \frac{\partial^2 u_x}{\partial x^2} + \nu \frac{\partial^2 u_x}{\partial y^2} + \nu \frac{\partial}{\partial x} (\nabla^2 \phi) \qquad (6)$$

The general similarity between Equation (6) and the boundary layer equation is obvious. If the boundary layer assumptions are applied to Equation (6), Equation (7) results:

$$W_x \frac{\partial u_x}{\partial x} + W_y \frac{\partial u_x}{\partial y} + u_x \frac{\partial^2 \phi}{\partial x^2} = \nu \frac{\partial^2 u_x}{\partial y^2} \qquad (7)$$

This transforms directly back into the familiar boundary layer equation by the substitution of Equation (5) for the potential gradient. It is well known that such an equation is parabolic; however, the introduction of streamwise diffusion changes this characteristic. The effect of streamwise diffusion can be observed by considering solutions to the following two linear equations:

$$\alpha \frac{\partial u}{\partial x} + \frac{\partial^2 u}{\partial y^2} = 0. \qquad (8)$$

$$\alpha \frac{\partial u}{\partial x} + \frac{\partial^2 u}{\partial x^2} + \frac{\partial^2 u}{\partial y^2} = 0. \qquad (9)$$

The solution to Equation (8) is given by Equation (10):

$$u = e^{\lambda^2 x/\alpha} \left[C_1 e^{\lambda y i} + C_2 e^{-\lambda y i} \right] \qquad (10)$$

The solution to Equation (9) is given by Equation (11):

$$u = \left(e^{-\beta x} + A e^{-\sigma x} \right) \left(e^{\lambda y i} + C_2 e^{-\lambda y i} \right) \qquad (11)$$

$$\beta = \frac{\alpha}{2} \left[1 + \sqrt{1 + 4 \lambda^2/\alpha^2} \right]$$

$$\sigma = \frac{\alpha}{2} \left[1 - \sqrt{1 + 4 \lambda^2/\alpha^2} \right]$$

For a well-posed initial value problem, the solution at x must be bounded. This is clearly so for Equation (8) only when α is negative. Otherwise, there exists some arbitrarily large frequency, λ, that will cause an arbitrarily large solution at x. α being negative corresponds to the normal viscous flow case without separation.

Independent of α, however, Equation (9) cannot be represented as an initial value problem. One coefficient or the other (σ or β) is always positive. Dodge and Lieber (Reference 2), using the stability theory of Warming and Hyett (Reference 3), show that the direct consequence of such a non-well-posed problem is that no consistent, stable forward-marching method exists using finite-difference operations. In forward flow, the number of steps to an obvious instability strongly depends on the magnitude of α. However, even though observable instabilities may not be present, the inclusion of streamwise diffusion into the difference operator serves no purpose, since it cannot result in increased accuracy.

For high Reynolds number flows where streamwise diffusion is small, the obvious assumption is to neglect its effect. This assumption has been applied beyond the boundary layer by Dodge (Reference 1) and Pratap et. al. (Reference 4). In the boundary layer at Reynolds numbers such that the boundary layer thickness is small compared to axial dimensions, neglect of the effect is a very good assumption. Figure 1 shows, as an example, the balance of a number of terms in the momentum equation for a case of a linear decrease in free-stream velocity. All terms result from a boundary layer finite-difference solution. The streamwise correction was, of course, not used in the differential equation, but calculated as an after result.

Although streamwise diffusion is small in the boundary layer, neglect of it may not be justified in a separated region. A great deal depends on the length scales involved, and generalizations are difficult. If the length of a separated bubble is similar in size to its width, streamwise diffusion would conceivably play a significant role. Because the bubble dimensions are strongly influenced by geometric as well as Reynolds number considerations, a general method for solution with imbedded, separated bubbles may well require the inclusion of streamwise diffusion in the momentum balance.

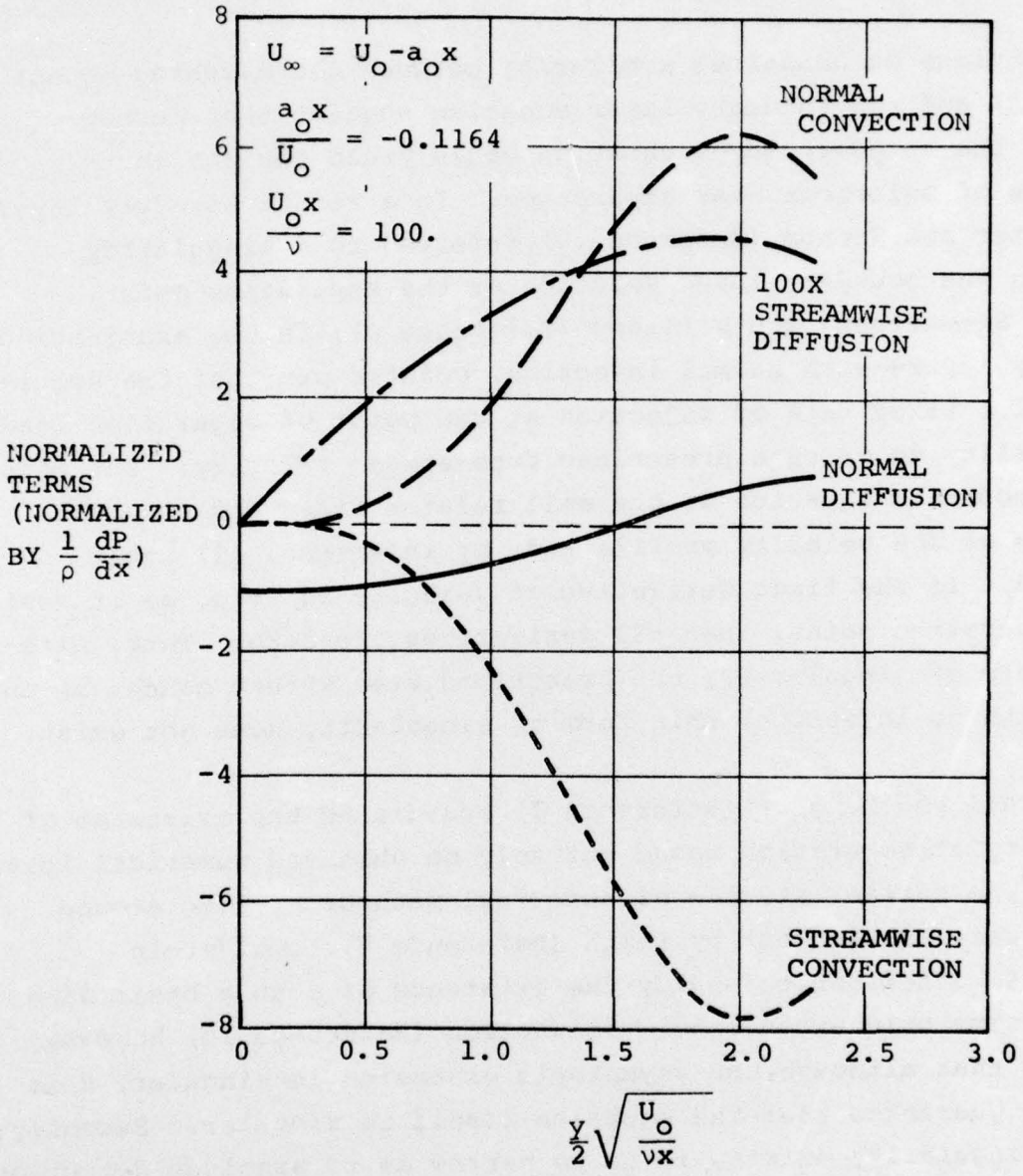

Figure 1. Comparison of Terms Through the Boundary Layer.

3.0 AT THE SEPARATION POINT

The obvious mathematical similarity between the marching equation, Equation (3), and the boundary layer equation suggest that perhaps a study of the boundary layer equation would yield insight to the performance of solutions near separation. In a recent boundary layer study, Carter and Wornom (Reference 5) referred to a singularity existing in the boundary layer solution at the separation point. Catherall, Stewartson, and Williams (Reference 6), in the examination of boundary layers with normal injection, pointed out that the specification of a fixed rate of injection at the point of separation leads to an inability to match a prescribed free-stream velocity. For this case, the momentum equation at the wall relates first and second derivatives of the velocity profile and, by inference, all other derivatives. If the first derivative of velocity is zero, as it must be at a separation point, then all derivatives are zero. Thus, without some form of singularity, the prescribed free stream cannot be met. However, with no injection, this form of singularity does not exist.

Catherall and Mangler (Reference 7) postulated the existence of a singularity at separation based entirely on observed numerical instabilities. The earlier studies of numerical methods applied around separation were carried out by Leigh (Reference 8). Goldstein (Reference 9) attempted to verify the existence of such a basic singularity by asymptotic expansions. Stewartson (Reference 10) however, pointed out that although the asymptotic expansion is singular, this provides no guarantee that the equation itself is singular. Secondly, if such a singularity exists, it is so narrow as to preclude detection by normal numerical methods. In addition, the above numerical studies did not take into account the fact that, in the separated bubble, the boundary layer equation is a non-well-posed initial value problem and, without modification, should not be soluble by any forward-marching method.

Still, the region around separation is extremely critical to the numerical technique proposed herein. The solution proposed for Equation (3) is similar to that of the boundary layer equation in that, through ϕ, a prescribed pressure field is imposed; however, it is different in that continuity is solved externally to the marching equation. Consequently, a numerical study utilizing the boundary layer equations was undertaken to observe the instabilities in and around the separation point.

The solution method was a basic implicit method similar to that described by Schlichting (Reference 11). The free-stream velocity was prescribed as linearly decreasing with distance along the plate, x. Ahead of separation, the solution proceeds in a normal fashion. Downstream of separation, however, the following assumptions were introduced in the back flow region in an attempt to produce a stable solution.

Case A. No change
Case B. No convection parallel to the wall
Case C. No convection parallel or normal to the wall
Case D. No convection parallel to the wall. Normal velocity set to zero
Case E. Normal velocity set to zero.

The above assumptions only apply to the regions where backflow occurs. Instabilities were not noted until they became obvious. As discussed in the previous section, Case A should be unstable. The elimination of free stream convection, B, removes the obvious problem of the momentum equation being non-well-posed. However, the normal component of velocity still has upstream influence through the continuity equation. The elimination of both normal and parallel convection should completely eliminate the difficulty with the momentum equation. The results for the first three cases (A, B, and C) were an obvious instability by about 10 percent (of the length to the separation point) downstream of the separation point.

Removing the objectionable terms from the momentum equation had little noticeable effect on the results. Case B, when applied to Equation (3) by Dodge (Reference 1) did, however, eliminate all observed numerical instabilities. The obvious difference is that the boundary layer equations include a continuity equation with upstream influence where the equations of Dodge do not. Consequently, Cases D and E were tried. Case D eliminates the objectionable continuity and parallel convection terms. Case E is included as a check case in which continuity is removed but parallel convection is not. The results were as follows:

Case D: No obvious instability within at least 100 percent of the separation length downstream.

Case E: Obvious instability at about 10 percent downstream of the separation point.

The success of Case D indicates that if the numerical problems created by backflow can be overcome, a solution for an arbitrarily imposed potential and thereby pressure gradient is obtainable. Ignoring parallel convection is, however, a suitable assumption only if the backflow region is sufficiently small. Streamwise convection can rapidly become significant as indicated by Figure 2. Streamwise convection is calculated from the results of Case D. Even though the point in question is only slightly downstream of the separation point, free-stream convection can hardly be ignored. This, then, leads to the numerical methods described in the following section.

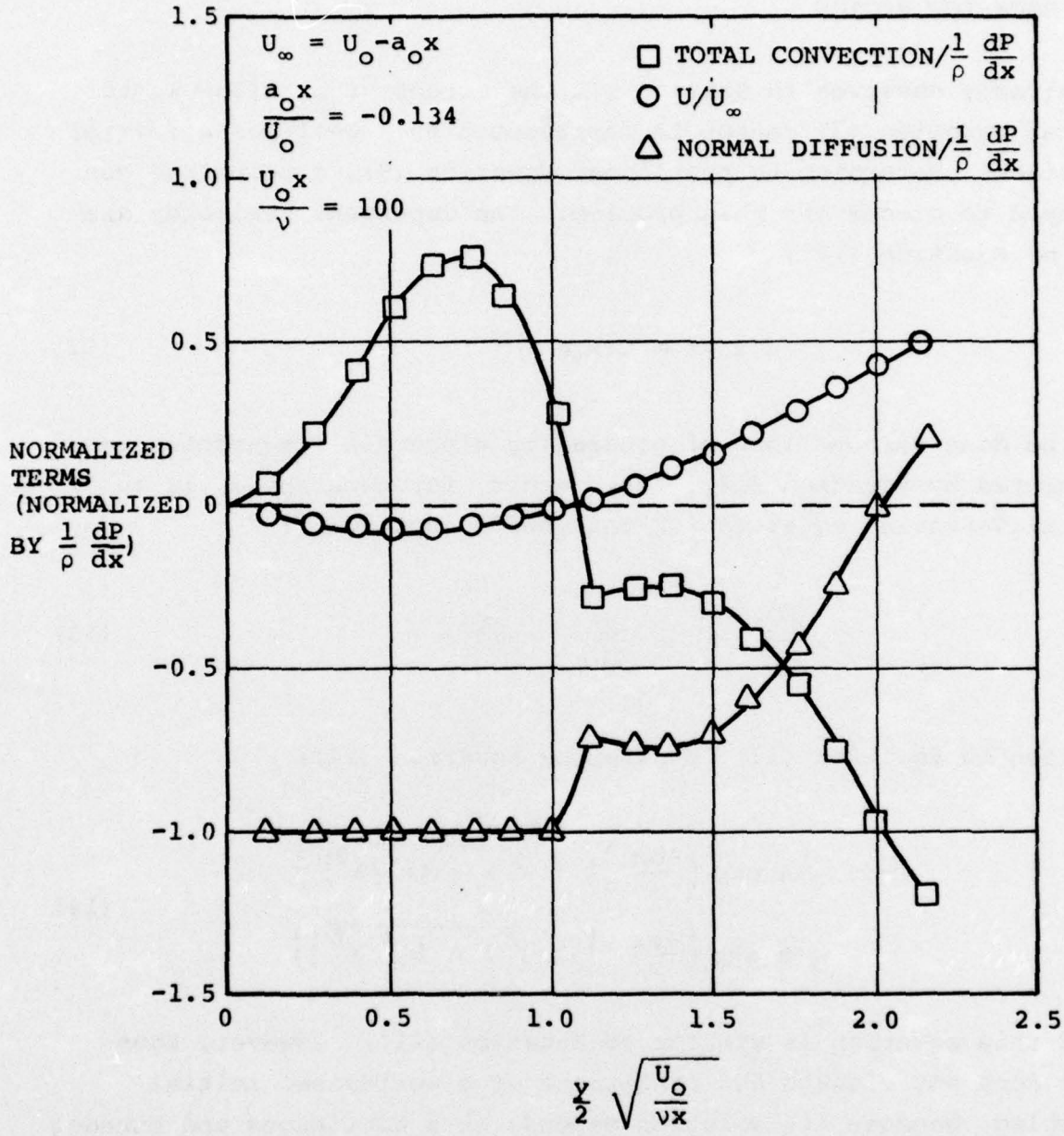

Figure 2. Comparison of Terms by Momentum Balance Through the Boundary Layer Method of Solution D.

4.0 THE BACKFLOW REGION

As already observed in Section II, the effect of backflow is to assure that Equation (3) cannot be represented as a well-posed initial value problem. Returning to the linear Equation (9), a technique can be developed to circumvent this problem. The dependent variables are replaced by Equation (12):

$$u(x,y) = C(x)e^{i\omega y} \tag{12}$$

This can be done without loss of generality since all frequencies can be represented by Equation (12). The result, for constant α, is an ordinary differential equation for the coefficient, C(x):

$$\frac{d^2C}{dx^2} + \alpha \frac{dC}{dx} - \omega^2 C = 0. \tag{13}$$

The solution to Equation (13) is given by Equation (14):

$$\begin{aligned} C(x) = A \exp\left(\frac{-\alpha x}{2}\left[1 + \sqrt{1 + 4\omega^2/\alpha^2}\right]\right) \\ + B \exp\left(\frac{-\alpha x}{2}\left[1 - \sqrt{1 + 4\omega^2/\alpha^2}\right]\right) \end{aligned} \tag{14}$$

Note that this equation is similar to Equation (11). However, Equation (14) does not violate the conditions of a well-posed initial value problem, because its solution depends in a continuous and bounded fashion on the initial conditions (a) and (b). Following the nomenclature of Richtmyer and Morton (Reference 12), if the solution to an initial value problem can be represented by a transformation given by Equation (15), then the following conditions are required for the problem to be well posed:

(a) $E_o(x)$ is continuous

(b) $E_o(x)$ is uniformly bounded--i.e.,

$$\| E_o(x) \| \leq K \text{ for } x_{min} \leq x \leq x_{max}$$

where K must be a finite constant

$$u(x) = u_o E_o(x) \tag{15}$$

Equation (9) violates condition (b), whereas Equation (13) on the other hand does not violate condition (b). Only a single finite frequency is being considered; thus, $E_o(x)$ is uniformly bounded, and stable forward-marching, finite-difference operations consistent with Equation (13) can be found.

This leads directly to consideration of such a technique applied to the more complicated non-linear equations of marching. Equation (3) expressed in a two-dimensional curvilinear coordinate system can be represented by Equation (16):

$$A_o u + A_1 \frac{\partial u}{\partial x_1} + A_2 \frac{\partial u}{\partial x_2} + A_{11} \frac{\partial^2 u}{\partial x_1^2} + A_{22} \frac{\partial^2 u}{\partial x_2^2} + s = 0 \tag{16}$$

In this case, only one of the dependent variables is shown, u representing either u_1 or u_2, depending on the situation. Additionally, the coefficients of the equation are non-linear functions of u_1, u_2, x_1, and x_2.

The dependent variable can be represented by an infinite series of a sufficiently general set of functions:

$$u(x_1, x_2) = C_o(x_1) g_o(x_2) + \sum_{n=1}^{\infty} C_n(x_1)\, g_n(x_2) \tag{17}$$

Substitution of Equation (17) into (16) yields Equation (18):

$$\sum_{n=1}^{\infty} \left(A_o C_n g_n + A_1 C_n' g_n + A_2 C_n g_n' + A_{11} C_n' g_n + A_{22} C_n g_n'' \right)$$

$$= -s - A_o C_o g_o - A_1 C_o' g_o - A_2 C_o g_o' - A_{11} C_o'' g_o$$

$$- A_{22} C_o g_o'' \qquad (18)$$

Treating the zeroth function separately allows it to be chosen to match exactly the boundary conditions resulting in simpler numerical solutions.

During the course of the study, several methods for obtaining the unknown coefficients were attempted. Dodge and Lieber (Reference 2) describe these developments. Two are noteworthy enough to be described herein.

The first, which will be referred to subsequently as the least squares method, represents only an approximate solution to the unknown coefficients. Each set of terms in Equation 18 may be equated to a function $e_n(x_1, x_2)$ representing an error, as follows:

$$A_o C_n + A_1 C_n' + A_2 C_n g_n'/g_n + A_{11} C_n'' + A_{22} C_n g_n''/g_n$$

$$+ d_n = e_n(x_1, x_2) \qquad (19)$$

Then the term is given by:

$$s = \sum_{n=1}^{\infty} d_n g_n + d_o g_o$$

If the right-hand side was identically zero for all n, then an exact solution would be obtained. Note, however, that this is not the only

way a solution can be reached. The other way is for e_n to be non-zero for a particular value of n, but canceled by other frequency components. The type of solution depends on the series choice and the problem type.

If the error e_n is approximated at a discrete number of points M, in the x_2 direction, then a total squared deviation parameter is defined by Equation (20):

$$E_n = \sum_{m=1}^{M} e_n^2 \tag{20}$$

The solution nearest the identically zero solution could be obtained by minimizing, E_n, the sum of the squares. To do this, the unknown coefficients are expanded in difference equations as indicated by Equation (21):

$$\frac{A_{11}}{\Delta x_1^2}\left[C_n^{(k)} - 2C_n^{(k-1)} + C_n^{(k-2)}\right] +$$

$$\frac{A_1}{2\Delta x_1}\left[3\,C_n^{(k)} - 4\,C_n^{(k-1)} + C_n^{(k-2)}\right] +$$

$$C_n^{(k)}\left[A_2 f_n'/f_n + A_{22} f_n''/f_n + A_o\right] + d_n = e_n \tag{21}$$

where:

$$x_1 = x_{1_o} + k\Delta x_1$$

Collecting terms in Equation (21), a simple relation for the unknown coefficient $C_n^{(k)}$ is obtained.

$$B_m C_n^{(k)} - \rho_m = e_n \tag{22}$$

where:

$$B_m = A_{11}/\Delta x_1^2 + \frac{3A_1}{2\Delta x} + A_2\, g_n'/g_n + A_{22} g_n''/g_n + A_o$$

$$\rho_m = C_n^{(k-1)} \left[\frac{2A_{11}}{\Delta x_1^2} + \frac{2A_1}{\Delta x_1}\right] - C_n^{(k-2)} \left[\frac{A_{11}}{\Delta x_1^2} + \frac{A_1}{2\Delta x_1}\right] - d_n^{(k)}$$

Differentiation of Equation (20) by the unknown coefficient, $C_n^{(k)}$, results in an evaluation of $C_n^{(k)}$ yielding the least square error:

$$C_n^{(k)} = \frac{\sum_{m=1}^{M} \rho_m B_m}{\sum_{m=1}^{M} B_m^2} \tag{23}$$

Solutions to Equation (24) were obtained utilizing this technique:

$$(W_\infty + u)\frac{\partial u}{\partial x} = \nu \frac{\partial^2 u}{\partial x^2} + \frac{\partial^2 u}{\partial y^2} \tag{24}$$

subject to the boundary conditions:

$$u(x,0) = -W_\infty$$

$$\frac{\partial^2 u}{\partial x^2}(x,\delta) = 0.$$

Since this is the equation for flow over a flat plate with no pressure gradient, backflow solutions were obtained by marching downstream and then reversing the process in an attempt to recover initial conditions. Simultaneous solutions were made with conventional finite-difference

methods. The finite-difference solution is compared to the least squares solution for the downstream marching in Figure 3. In the reverse direction, finite-difference solutions become obviously unstable within a few marching steps. Figure 4 displays the results of the least squares calculation. Note that the return solution is a close approximation to the initial conditions. Figure 5 shows the variation of spectral coefficients involved in this process. The series used is given by Equation (25):

$$u(x,y) = -W_\infty + \sum_{n=1}^{N} C_n(x) \sin\left((2n-1)y\ \pi/\delta\right) \qquad (25)$$

Note that the boundary conditions are automatically preserved by such a choice. Secondly, it is useful to observe the low number of functions actually utilized. It might be expected that such a limited set could not describe a turbulent boundary layer. However, the number of functions depends on which functions are used, and the orthogonal transformation applied to the grid system. As will be seen in a later section, good results can be obtained with only a modest number of coefficients, even for a very complicated situation.

Such a least squares method is suitable for obtaining insight into the method, and showing its capability to solve backflow problems. However, it is not practical for more complicated situations involving pressure gradients and curvilinear geometries. Dodge and Lieber (Reference 2) show that the simple addition of a pressure gradient to Equation (24) results in large solution errors by the least squares method. Consequently, the following method was developed.

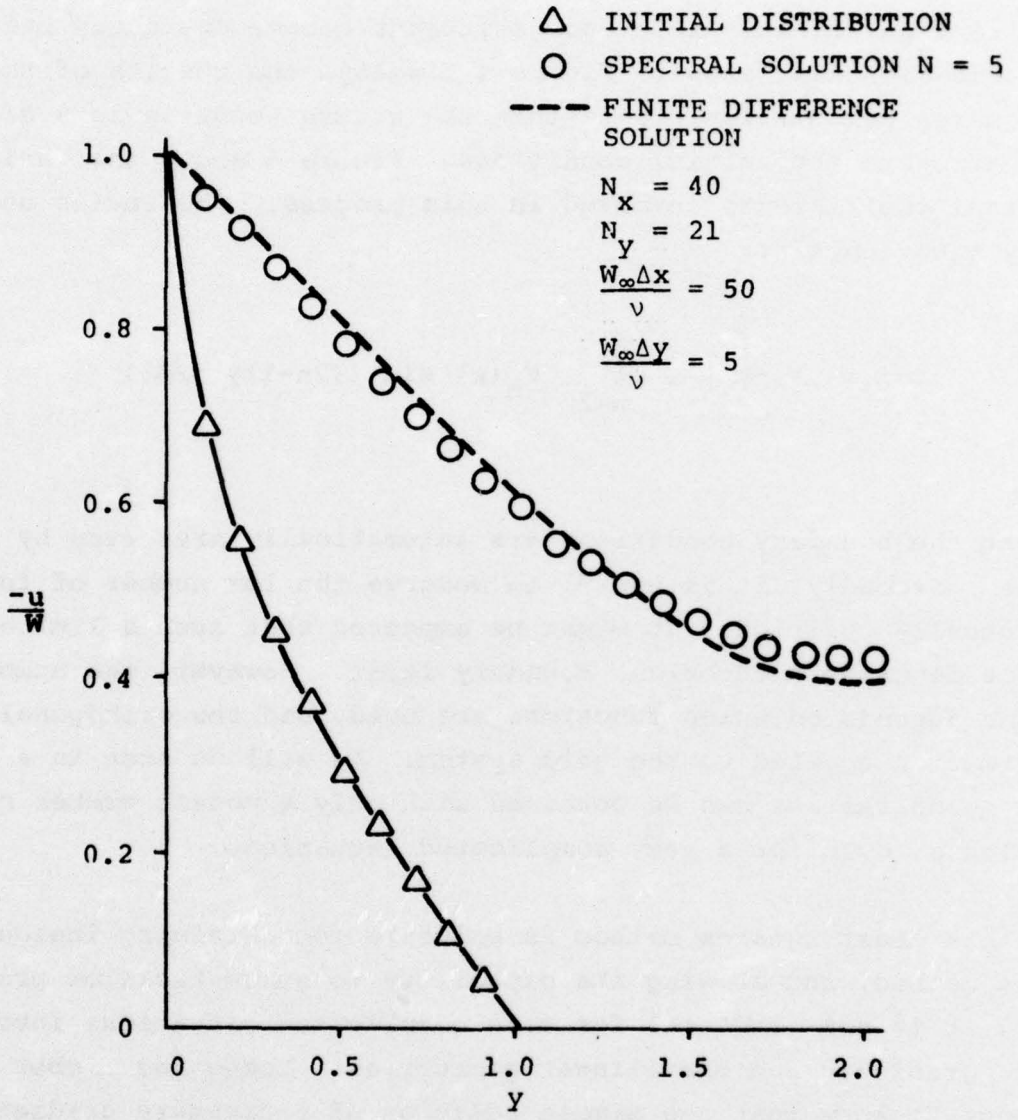

$$\frac{W}{\nu}\frac{\partial u}{\partial x} = \frac{\partial^2 u}{\partial x^2} + \frac{\partial^2 u}{\partial y^2}$$

$$W = W_\infty + u$$

Figure 3. Comparison of Numerical Solutions to Forward Flow.

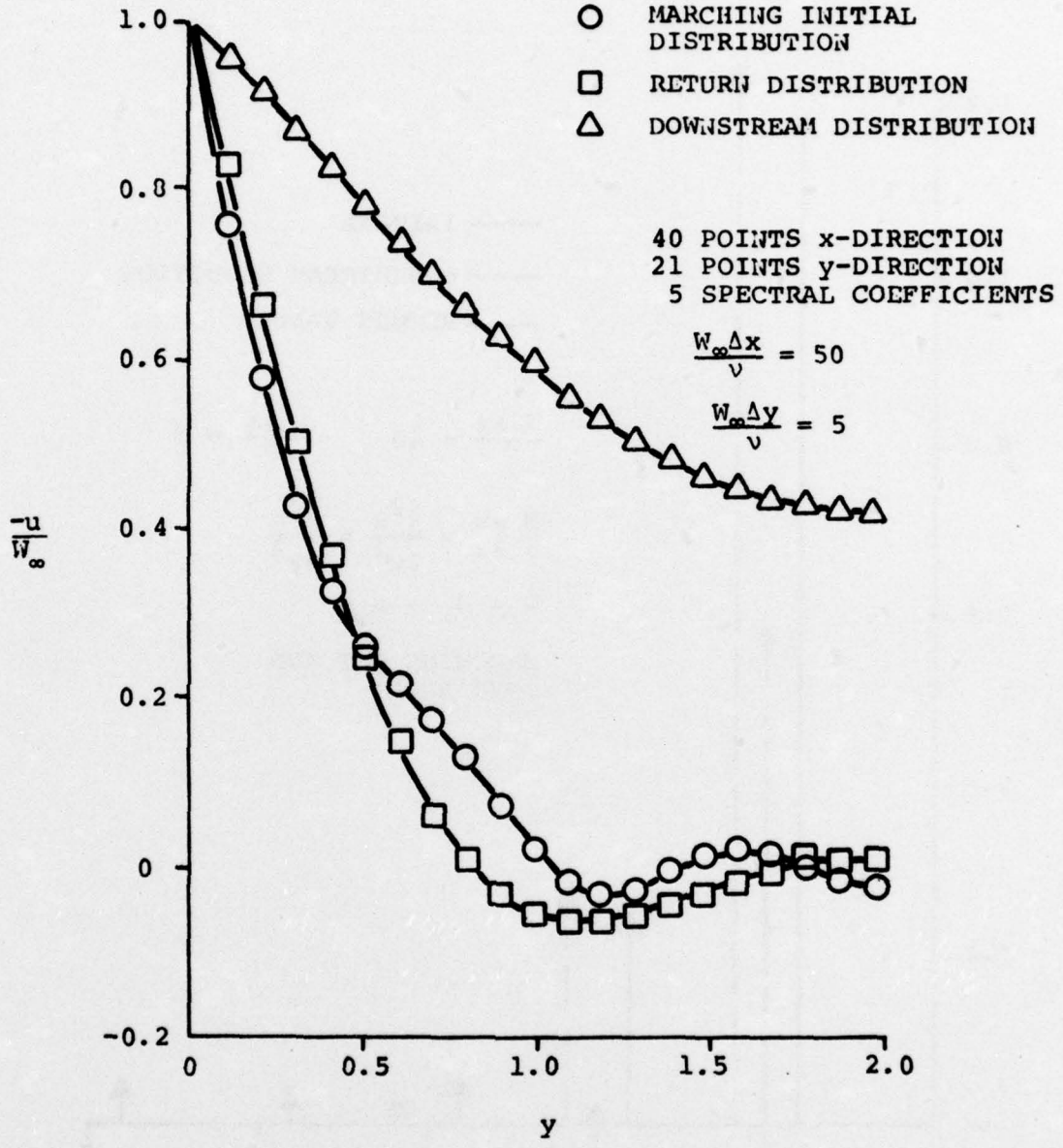

Figure 4. Spectral Solution Marching Forward Then Back to Starting Point.

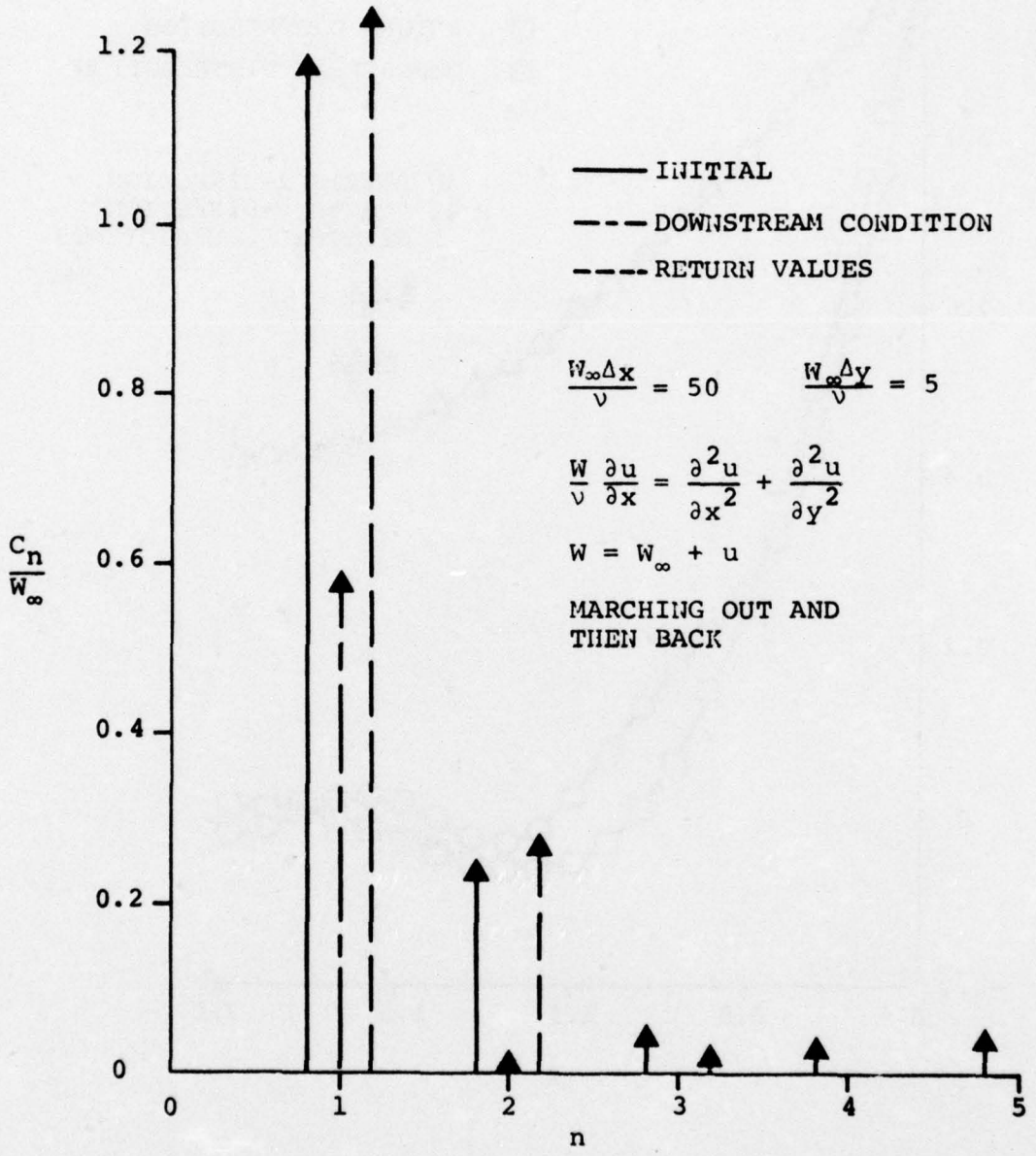

Figure 5. Spectral Coefficients.

5.0 METHOD OF WEIGHTED RESIDUALS

A better-based method of solution can be obtained by multiplying Equation (18) by one member of the functional set, g_k, and then integrating over the solution region.

$$\sum_{n=1}^{\infty} \left\{ C_n \int_0^{\delta} (A_o g_n g_k + A_2 g_n' g_k + A_{22} g_n'' g_k)\, dx_2 + C_n' \int_0^{\delta} A_1\, g_n g_k\, dx_2 + C_n'' \int_0^{\delta} A_{11}\, g_r g_k\, dx_2 \right\}$$

$$= -\int_0^{\delta} s g_k\, dx_2 - C_o' \int_0^{\delta} A_1\, g_o g_k\, dx_2 - C_o'' \int_0^{\delta} A_{11} g_o g_k\, dx_2$$

$$-C_o \int_0^{\delta} (A_{22}\, g_o'' g_k + A_o g_o g_k + A_2 g_o'\, g_k)\, dx_2 \qquad (26)$$

The result, for a finite number of functions is a set of coupled ordinary differential equations for the unknown coefficients, C_n. If g_n and its derivatives are orthogonal over the interval $(0,\delta)$, and if the coefficients of the differential equation are not a function of x_2, the off-diagonal terms become zero and the equations decouple. The linear equation solution given by Equation (14) then falls out immediately. In general, with a non-linear curvilinear transformation to Equation (3), the off-diagonal terms of Equation (26) are not large and a reasonably non-singular matrix results. This technique is similar to several methods reported by Ames (Reference 13) for fluid dynamic problems.

The choice of function set can be somewhat artistic. The functional set was chosen so that the anticipated boundary conditions were met automatically. These conditions on the wall are given by Equations (27) and (28):

$$u_2\ (x_1,0) = -\frac{1}{h_2}\ \frac{\partial \phi\ (x_1,o)}{\partial x_2} = -V\ (x_2) \tag{27}$$

$$u_1(x_1,o) = 1/h_1\ \frac{\partial \phi\ (x_1,0)}{\partial x_1} \tag{28}$$

Either a zero value of u or a zero derivative of u was applied to the outer boundary depending on the series used.

The following functional sets were examined.

Set A - Sine Series

$$g_n(x_2) = \begin{cases} 1 & n=0 \\ \sin \lambda_n\ x_2 & n\neq 0 \end{cases}$$

$$\lambda_n = (2n-1)\ \pi/\delta$$

Set B - Modified Chebyshev Series

$$g_n\ (x_2) = T_n\ (y^*) + \sum_{k=1}^{3} d_k\ T_{n+k}\ (y^*)$$

where:

$$y^* = \frac{2x_2}{\delta} - 1.0$$

$T_n(y^*)$ = Chebyshev polynomial of order n

the coefficient d_k is chosen so that

$$g_o(o) = 1.0$$

$$g_n(o) = 0 \qquad n \geq 0$$

$$g_n(\delta) = 0 \qquad n \geq 0$$

$$g_n'(\delta) = 0 \qquad n \geq 0$$

Set C - Sine-Cosine Series

$$g_n(x_2) = \sin \lambda_n x_2$$

$$\lambda_n = \frac{n\pi}{\delta} \qquad n \geq o$$

$$g_o(x_2) = \cos \frac{\pi x_2}{\delta}$$

Set D - Poly Sine Series

$$g_o(x_2) = (1-x_2/\delta)^3$$

$$g_n(x_2) = \sin (n\pi x_2/\delta) \qquad n > o$$

Each of the above methods were compared against solutions to Equation (29):

$$W \frac{\partial u}{\partial x} + u \frac{d^2\phi}{dx^2} = \nu \frac{\partial^2 u}{\partial y^2} \tag{29}$$

where:

$$W = \frac{d\phi}{dx} + u$$

The boundary layer type equation corresponding to Equation (29) is given by Equation (30):

$$W \frac{\partial W}{\partial x} = -1/\rho \frac{dp}{dx} + \nu \frac{\partial^2 W}{\partial y^2} \tag{30}$$

A Pohlhausen-type solution was used for comparison. The Pohlhausen solution differs from that of Schlichting (Reference 11), however, in that no continuity equation is present. The development of this particular Pohlhausen solution is given by Dodge and Lieber (Reference 2) and will not be included here. Various amounts of diffusion and acceleration were applied. Initial conditions were based upon a Pohlhausen profile at a very small value of x.

Since the Pohlhausen solution is not exact, it cannot be compared directly, particularly for diffusing cases where the Pohlhausen solution predicts a larger displacement thickness than actually exists. The Pohlhausen solution is then used as verification of general trends, and internal comparisons must be made to differentiate somewhat imperfectly between methods.

The modified Chebyshev series illustrates the importance of the orthogonality or near-orthogonality in the function set. The motivation behind this set of functions rests in the fact that Chebyshev polynomials can be evaluated much more rapidly, due to the existence of an algebraic recursion relationship between successive Chebyshev polynomials. However, as a plot of the first three functions shows (Figure 6), the functions are far from orthogonal. They are sufficiently non-orthogonal that the resulting matrix is difficult-to-impossible to invert and no solutions were obtained.

The original choice of the function set was Set A. Set C was chosen since the cosine functions more closely approximate a boundary layer profile (varying from unity at $x_2=0$ to zero at $x_2=\delta$) than does the constant of Set A. Figures 7, 8, and 9 show the results for accelerating flow, and two points in decelerating flow. Figure 9 contains several solutions with differing spacing in an attempt to explore the convergence of the method. From the baseline, the step size in the x direction and then in the y direction was reduced. Higher accuracy solutions should proceed from squares to diamonds to triangles. It is not unreasonable to see such a trend toward higher accuracy, as indicated in Figure 9.

$$g_n = T_n(y^*) + \sum_{k=1}^{3} d_{k,n} T_{n+k}(y^*)$$

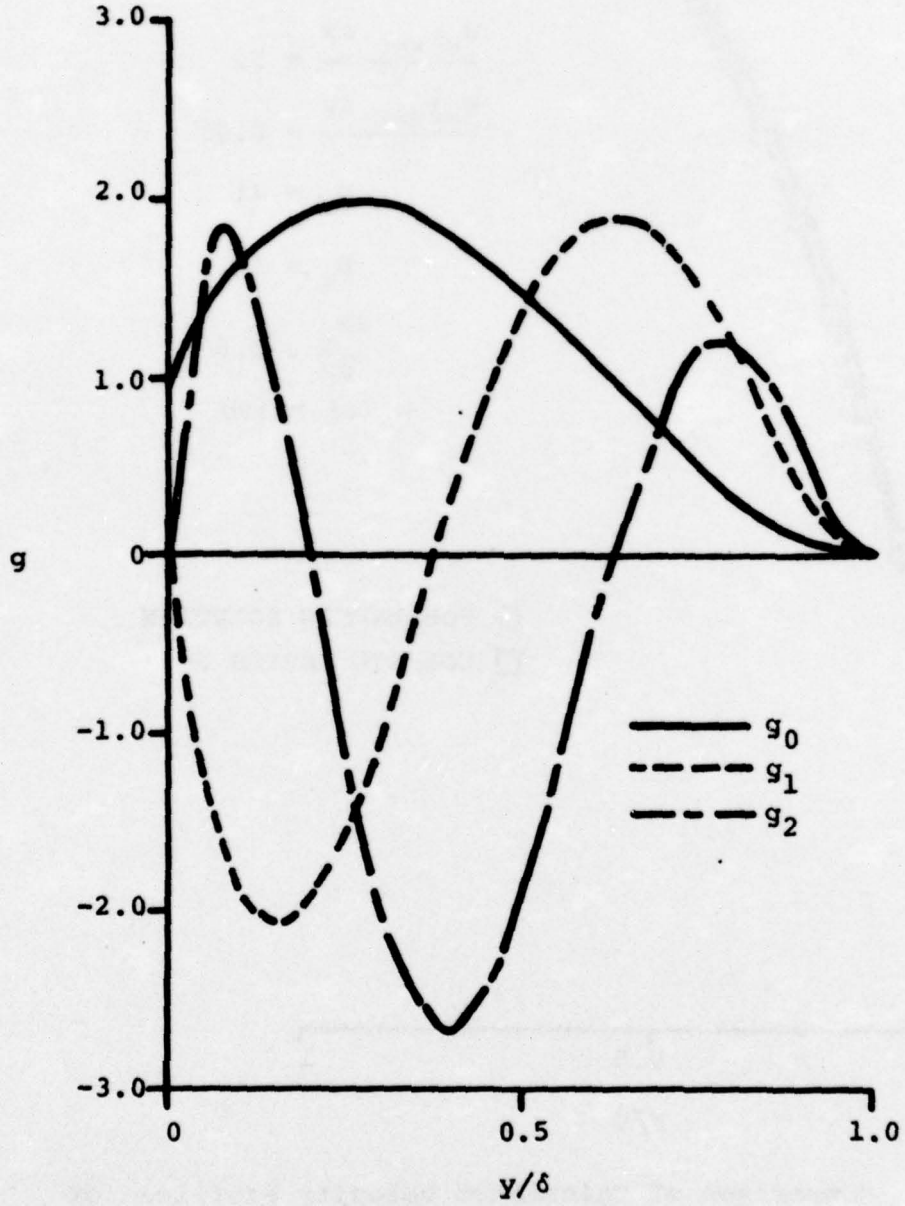

Figure 6. Grouped Chebyshev Functions.

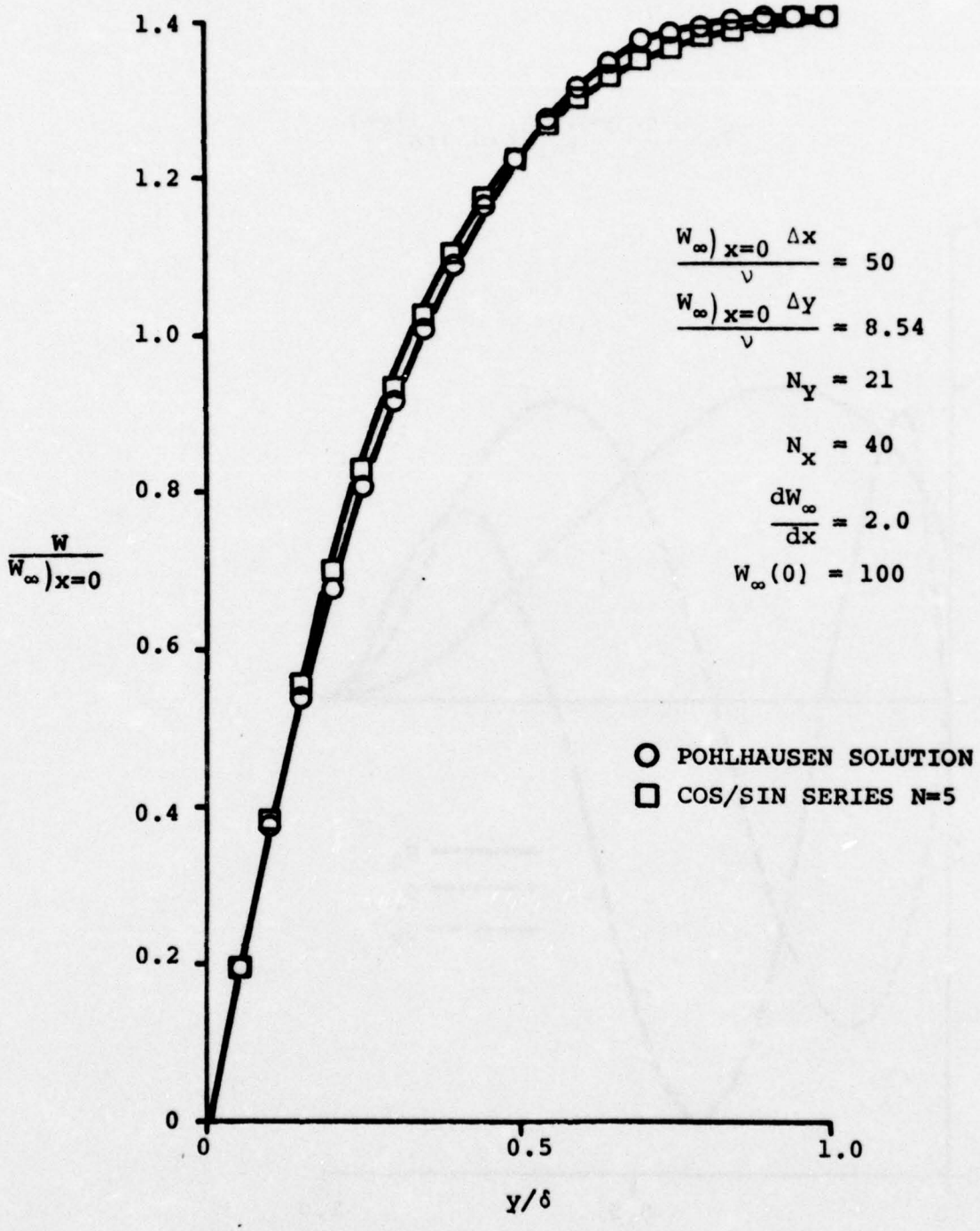

Figure 7. Comparison of Calculated Velocity Profiles for Accelerating Flow.

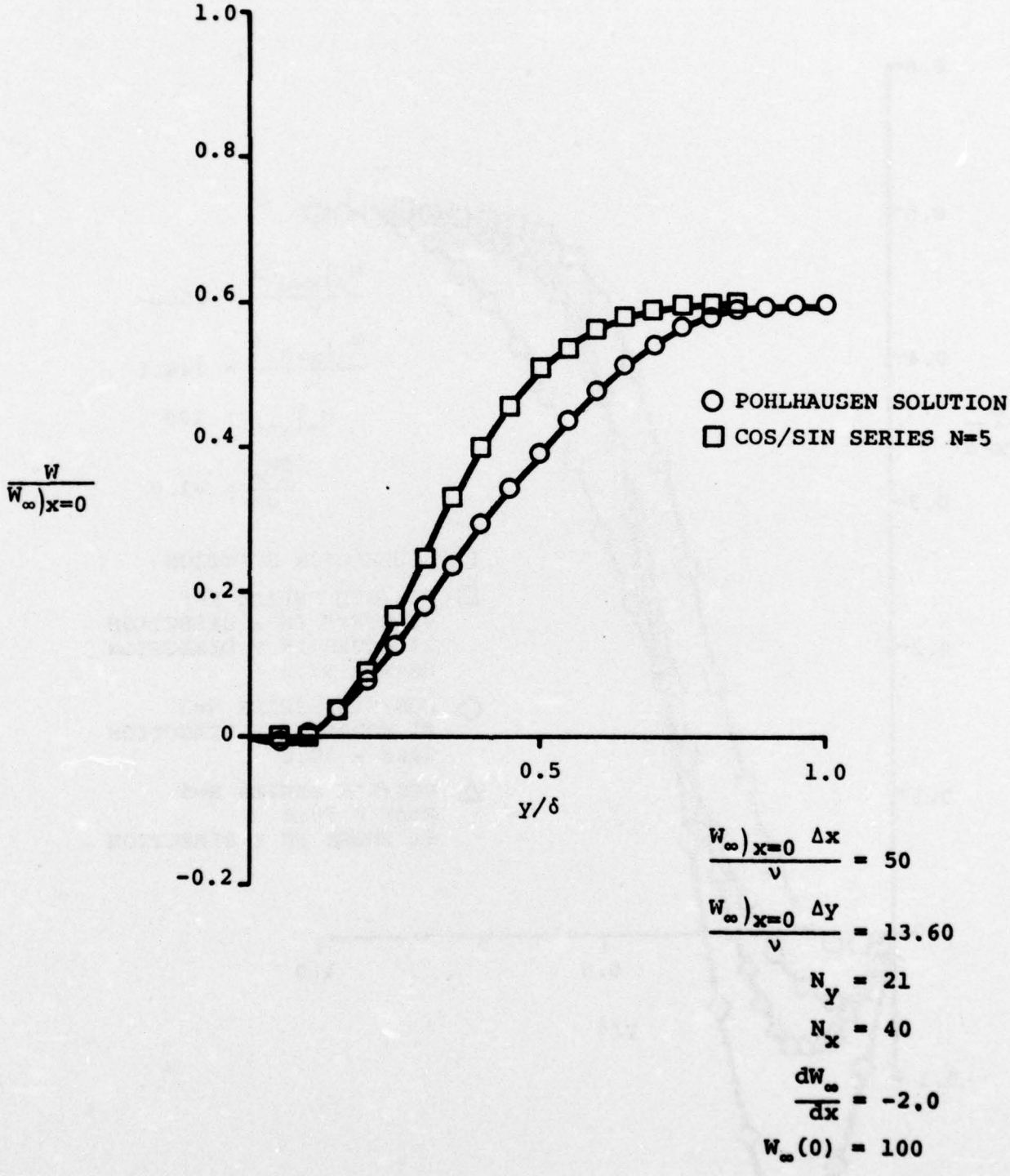

Figure 8. Comparison of Calculated Velocity Profiles for a Decelerating Flow.

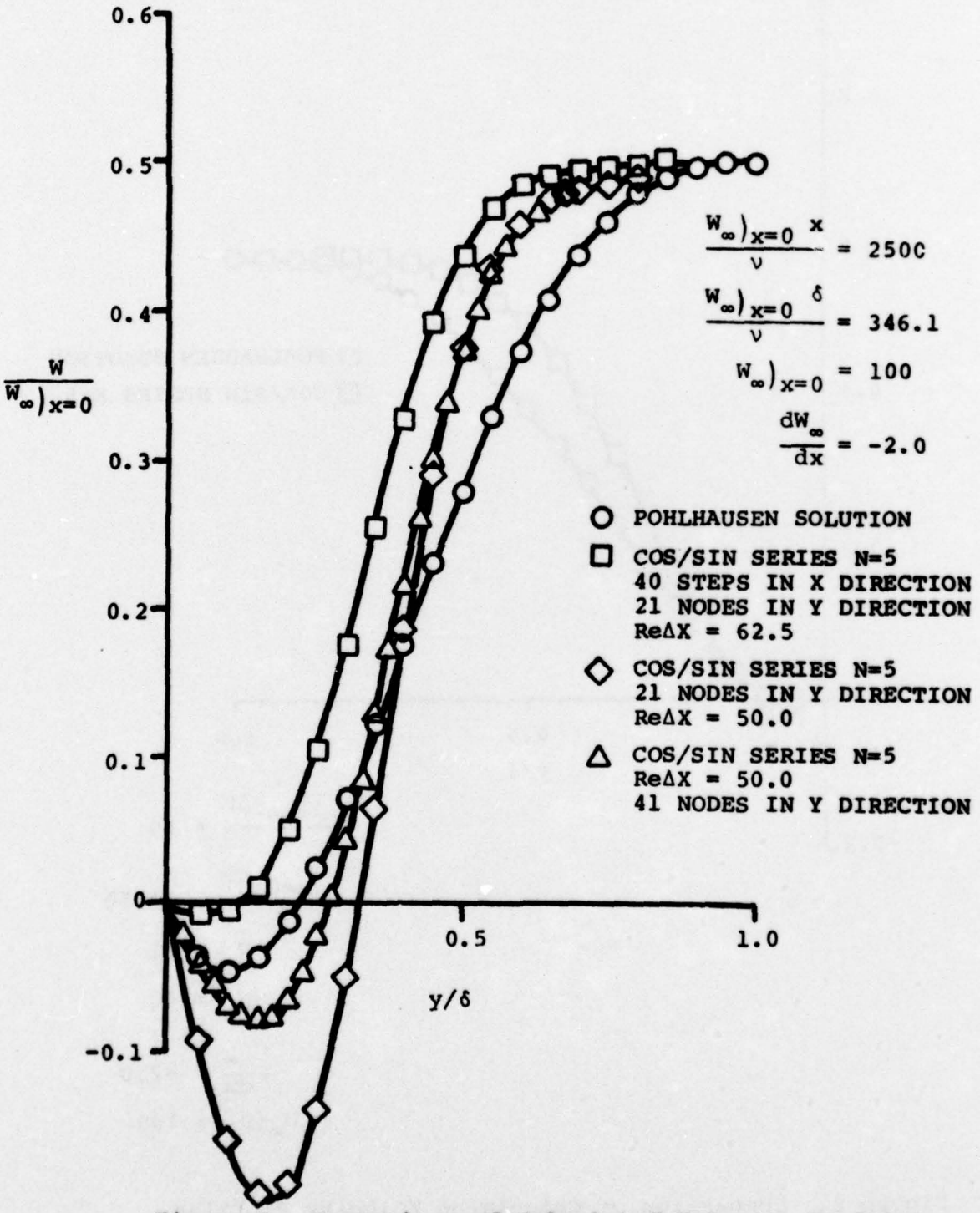

Figure 9. Comparison of Calculated Velocity Profiles.

The poly-sine series (Set D) was chosen to correct one deficiency in the sine-cosine series (Set C). The cosine has the wrong inflection across the boundary layer. The polynomial of Set D does not. Figures 10 and 11 show the results for accelerating and decelerating flow compared to Pohlhausen and Set C. Little significant difference between individual solutions was observed. However, the magnitude of first- and second-order coefficients sharply reduced between Sets C and D.

The sine series (Set A) was the original series (on a chronological basis). Figures 12 and 13 show comparisons between calculation methods for accelerating and decelerating flow. Again, little difference is observed. However, higher order coefficients are largest in magnitude with Set A.

The conclusions of the above study were: first, few differences between orthogonal function based methods (Set A, C, and D) were observed; second, it is important to have function sets that are orthogonal, or nearly so; and third, the general solution agrees with expectations. With this experience, a program to solve for the flow about an isolated body in a wind tunnel without sidewall boundary layers was undertaken.

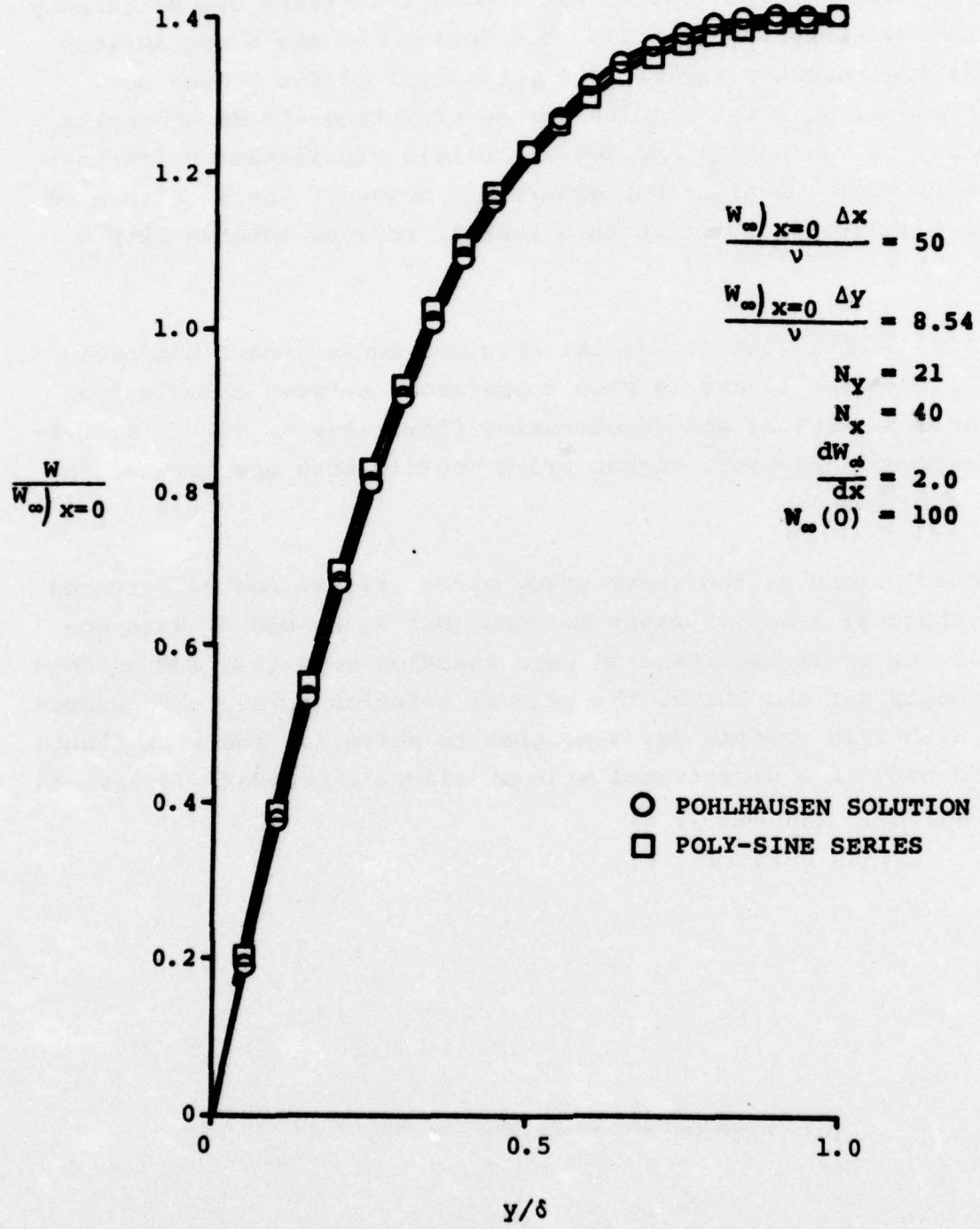

Figure 10. Comparison of Calculations for Accelerating Case.

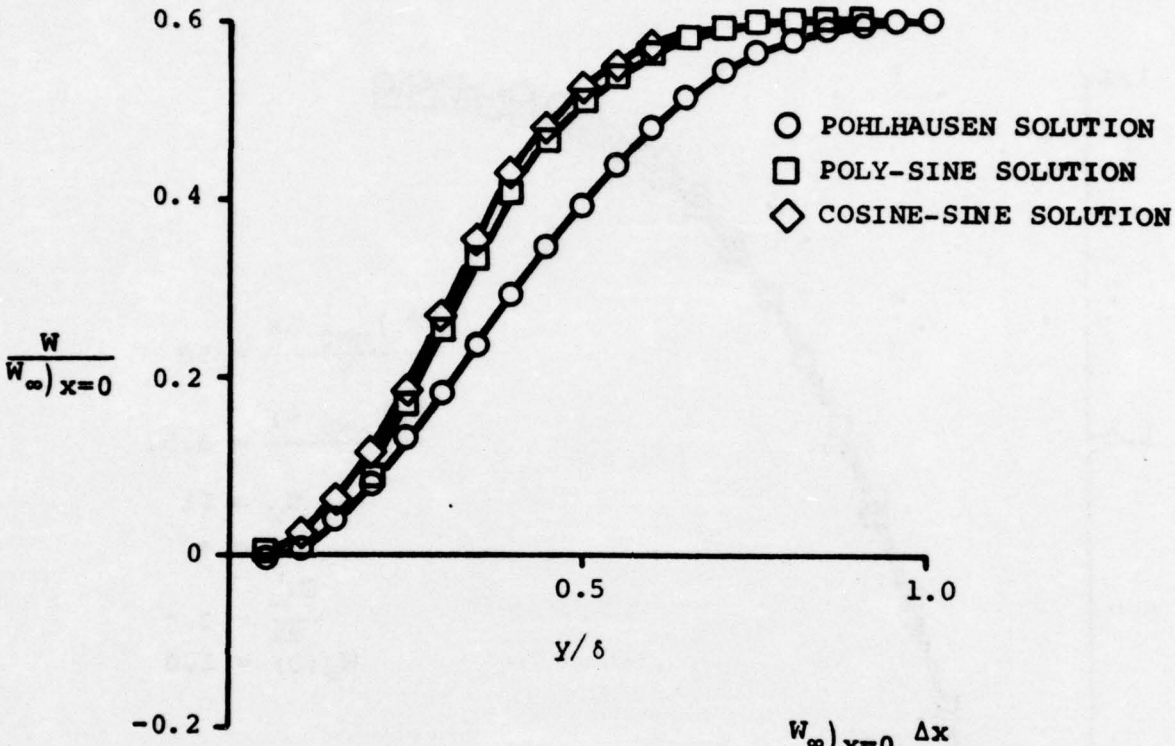

$$\frac{W_\infty)_{x=0}\,\Delta x}{\nu} = 50$$

$$\frac{W_\infty)_{x=0}\,\Delta y}{\nu} = 13.60$$

$$N_y = 21$$

$$N_x = 40$$

$$\frac{dW_\infty}{dx} = -2.0$$

$$W_\infty(0) = 100$$

Figure 11. Comparison of Calculations for Decelerating Case.

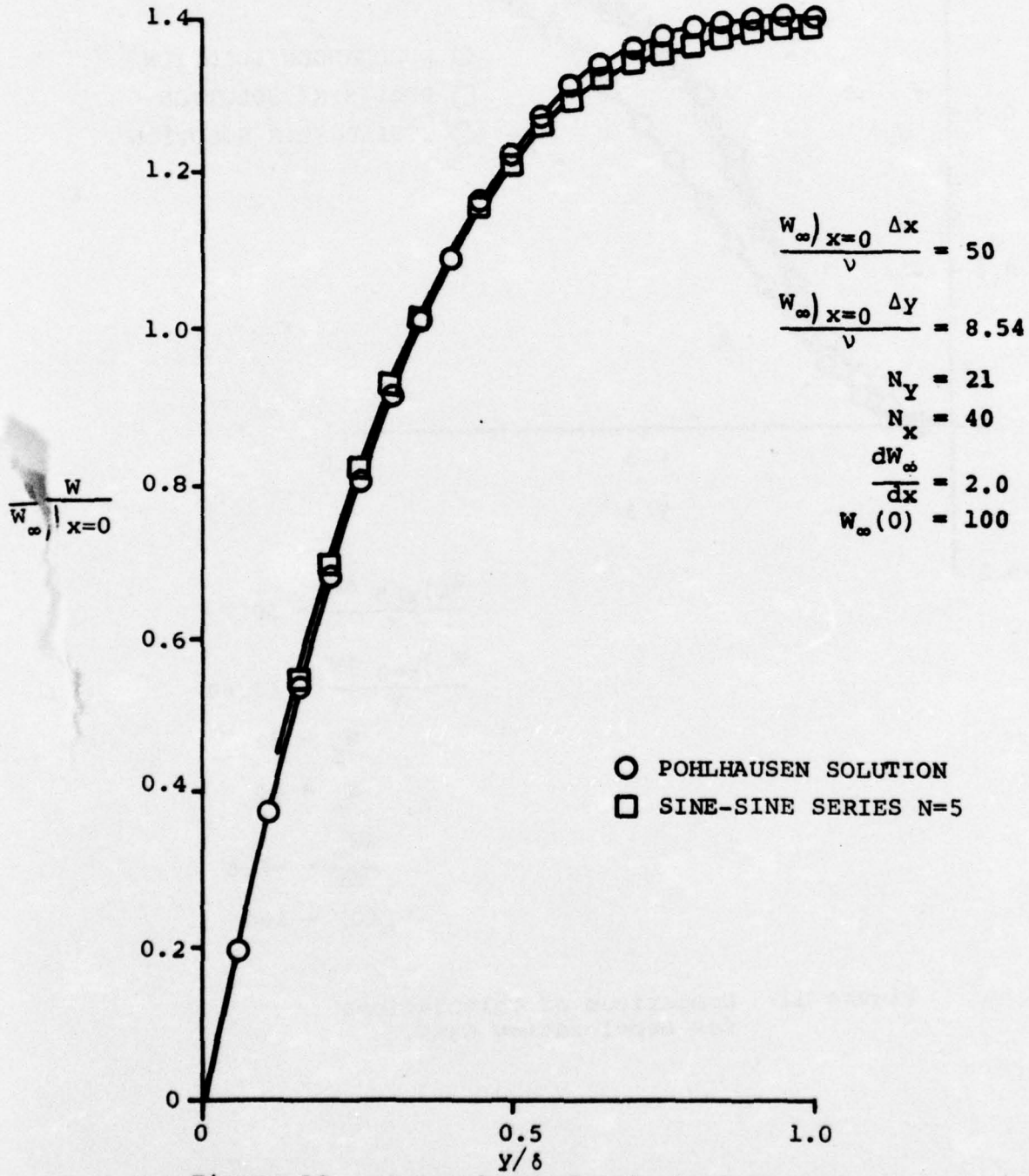

Figure 12. Comparison of Calculations for Accelerating Case.

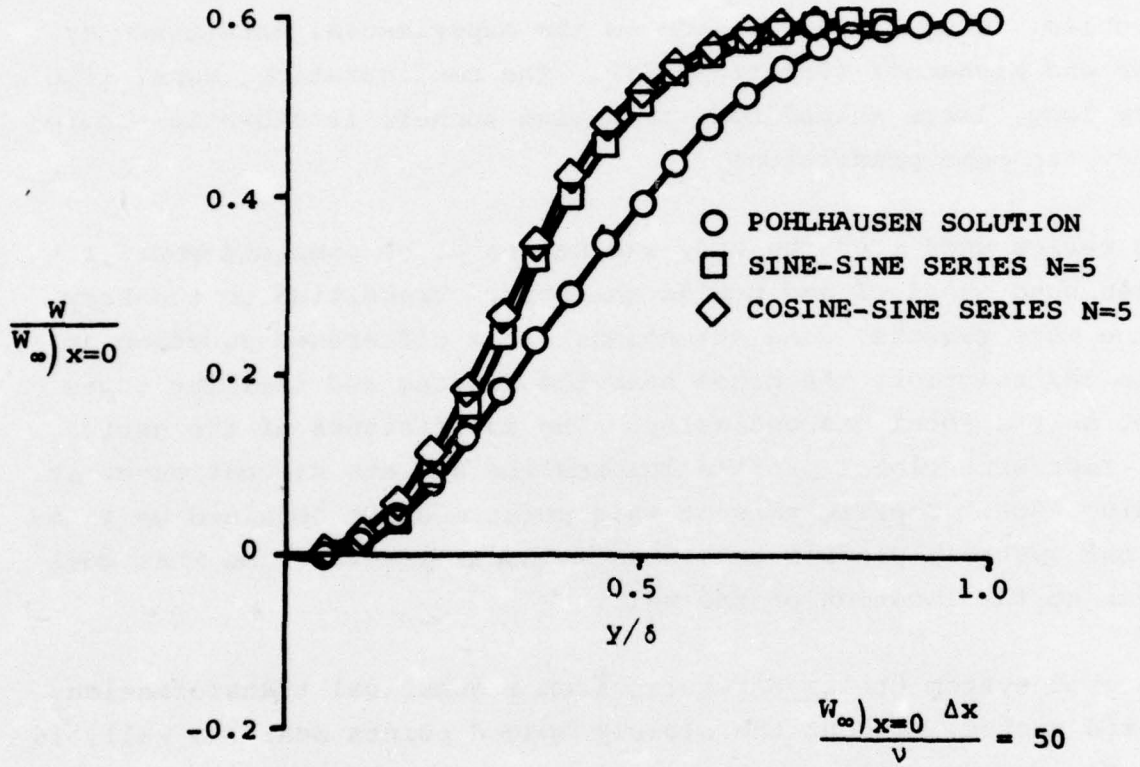

$$\frac{W_\infty)_{x=0}\,\Delta x}{\nu} = 50$$

$$\frac{W_\infty)_{x=0}\,\Delta y}{\nu} = 13.60$$

$$N_y = 21$$

$$N_x = 40$$

$$\frac{dW_\infty}{dx} = -2.0$$

$$W_\infty(0) = 100$$

Figure 13. Comparison of Original Series to Other Calculations.

6.0 COMPARISON TO DATA

A demonstration of the above method was undertaken for a full-scale problem. Comparison was made to the experimental data taken by Schubauer and Klebanoff (Reference 14). The configuration, consisting of a very long, large shaped body in a wind tunnel, is shown in Figure 14, along with some predictions.

The series used over the body was Series A. A complete Fourier series was used ahead of and behind the body. Transition to the body and to the wake requires some attention. In a difference equation approach to the solution, the nodes near the leading and trailing edges represent only a local discontinuity. The coefficients of the series, however, represent global profile information and are discontinuous at the leading edge. Coefficients at this point must be obtained by integrating the upstream profile to a discontinuous profile, one that goes to no-slip at the location of the wall.

The grid system utilized results from a numerical transformation. Such a grid system, without the closely spaced points near the wall, is shown in Figure 15. Wall points are placed at the users discretion. Good results have been obtained using a logarithmic spacing with a factor of several thousand between the smallest and largest increments. Something on the order of 20 points are used across the boundary layer with a like number across the rest of the tunnel passage. The relaxation solution was carried out on a sparse subset of the marching grid utilizing its own transformation coefficients.

The comparison between experiment and data in incompressible flow is sharply complicated by the need for a turbulence model. Needless to say, no agreement on an adequate model exists, especially when complicated by separated bubbles. As such, the comparison can only be used as further evidence of the reasonableness of the results. To this end, the basic turbulence model was essentially that utilized by

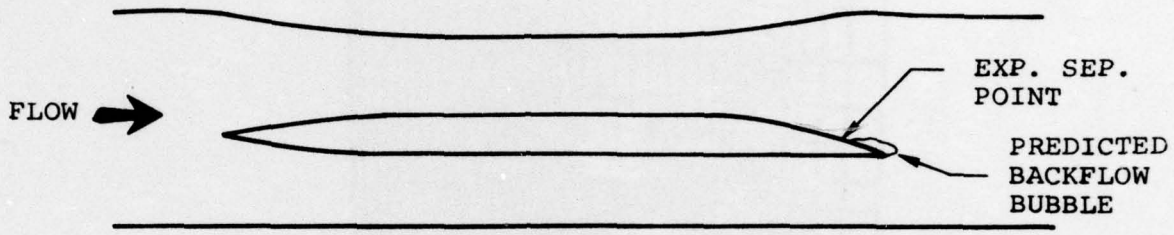

REYNOLDS NO. = 23 X 10^6

Figure 14. Shaped Body in Wind Tunnel.

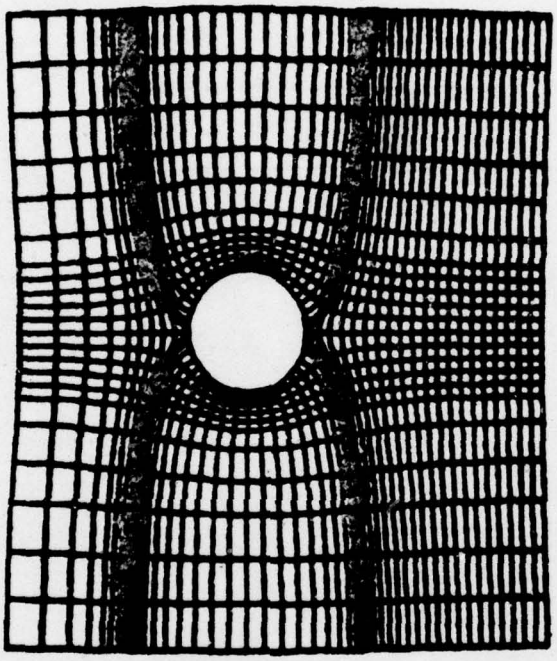

CIRCULAR CYLINDER IN CROSS FLOW RADIUS=1.0

Figure 15. Full Relaxation Grid.

Dodge (Reference 1) successfully in three-dimensional flows. This basic model is a mixing-length model with the mixing length modified by van Driest's (Reference 15) correction for wall shear and the Cebeci-Smith (Reference 16) correction for pressure-gradient effects on turbulence. The mixing length increases until a cutoff value is reached. This cutoff is a function of free stream turbulence. Dodge reports a cutoff at approximately 0.02 of chord for levels of turbulence consistent with internal flows. Comparisons to data were made at the trailing edge, and undoubtedly, significant error occurred near the leading edge. Although these values of ℓ_{max} are somewhat larger than those suggested by Launder and Spalding (Reference 17) they are representative of the values required to predict a fairly wide range of internal flows. The three following approximations were utilized for calculations on the Schubauer and Klebanoff configuration.

(1) A constant cutoff of $\ell_{max} = 0.585$ feet

(2) A variable cutoff with two different distributions (see Figure 16).

(3) An Alber cutoff on the value of kinematic viscosity at the edge of the boundary layer.

$$\upsilon_e = 0.0168\ W_e\ \delta^*$$

where: W_e is the edge velocity

δ^* is the displacement thickness.

Results for all three models are shown in Figure 17 for displacement thickness and Figure 18 for shape factor. As expected, the constant cutoff produced a too-rapid early growth with a too-slow growth near the trailing edge.

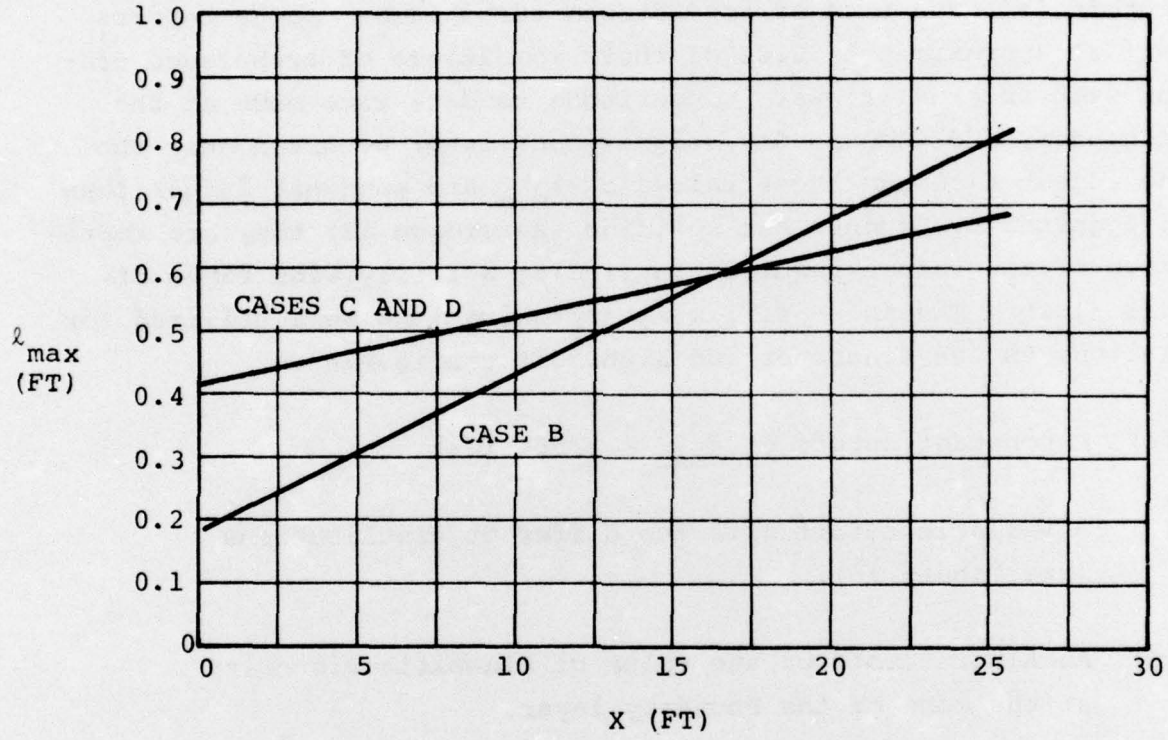

Figure 16. Variation of Maximum Mixing Length with Position - Model 2.

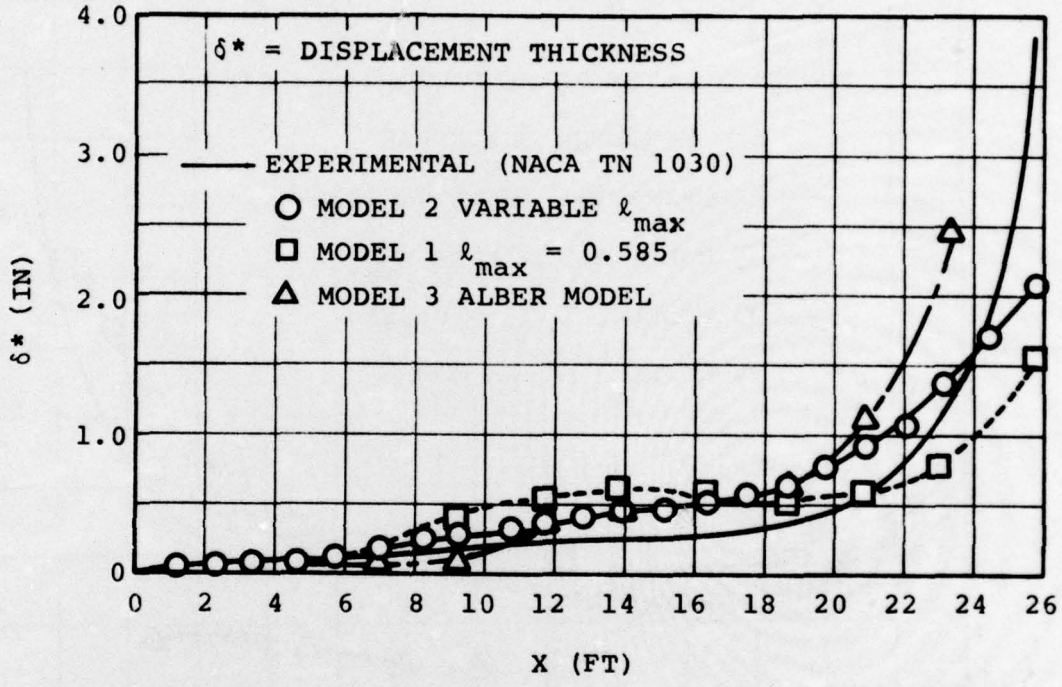

Figure 17. Comparison of Experimental and Calculated Displacement Thicknesses.

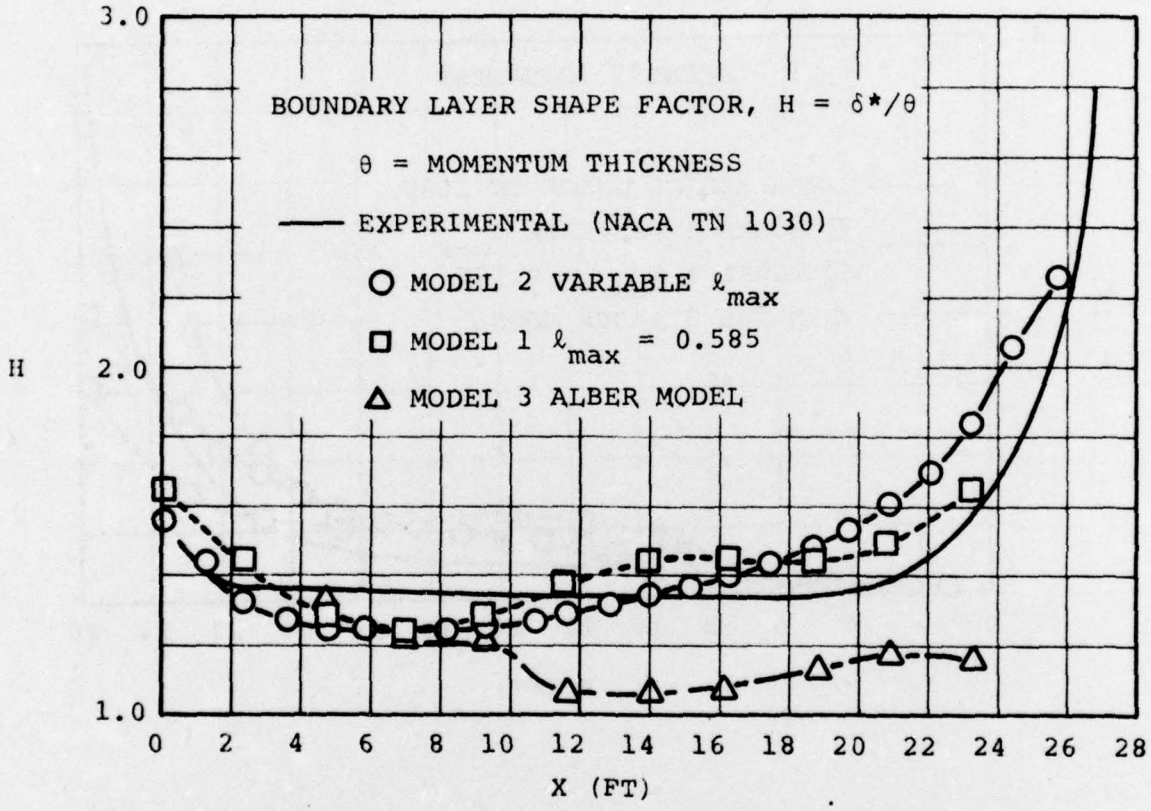

Figure 18. Comparison of Experimental and Calculated Shape Factor.

The variable cutoff does quite well, however. The Alber model suffers in a full Navier-Stokes solution with the need to define such nebulous quantities as the freestream velocity and the displacement thickness. The numerical method used resulted in an apparently spurious interaction between cutoff values and solutions, yielding the poor results shown. Undoubtedly, it was a problem that could be overcome, but it was judged not to be worthwhile to pursue it further. Figure 19 shows the separation points of the various techniques and a calculated separated bubble. An earlier separation, closely confined to the surface, is predicted by Model (2); however, the bubble for Model (2) has a reasonable position and size when compared to data.

Velocity profiles are shown for the following cases to illustrate the effect of successive passes through the relaxation equation (Equation 14) with various flavors of the first two turbulence models.

Case A 1 outer loop (one relaxation, one march), Model 1 with $\ell_{max} = 0.585$

Case B 1 outer loop, Model 2 with ℓ_{max} variable as specified by Figure 16.

Case C 1 outer loop, Model 2 with ℓ_{max} variable as specified by Figure 16.

Case D 3 outer loops (3 relaxations, 3 marches), Model 2 with ℓ_{max} variable as specified by Figure 16.

Only the calculation points in the outer boundary layer portion of the flow are shown. Additional points are closer to the wall and out in the channel. Figures 20, 21, 22, 23, and 24 compare profiles at discrete locations along the body. As can be expected, Case D offers a reasonable fit to data. The effect of iteration is most pronounced near the trailing edge where the separation region changes from iteration to iteration, indicating the importance of the static pressure in this region.

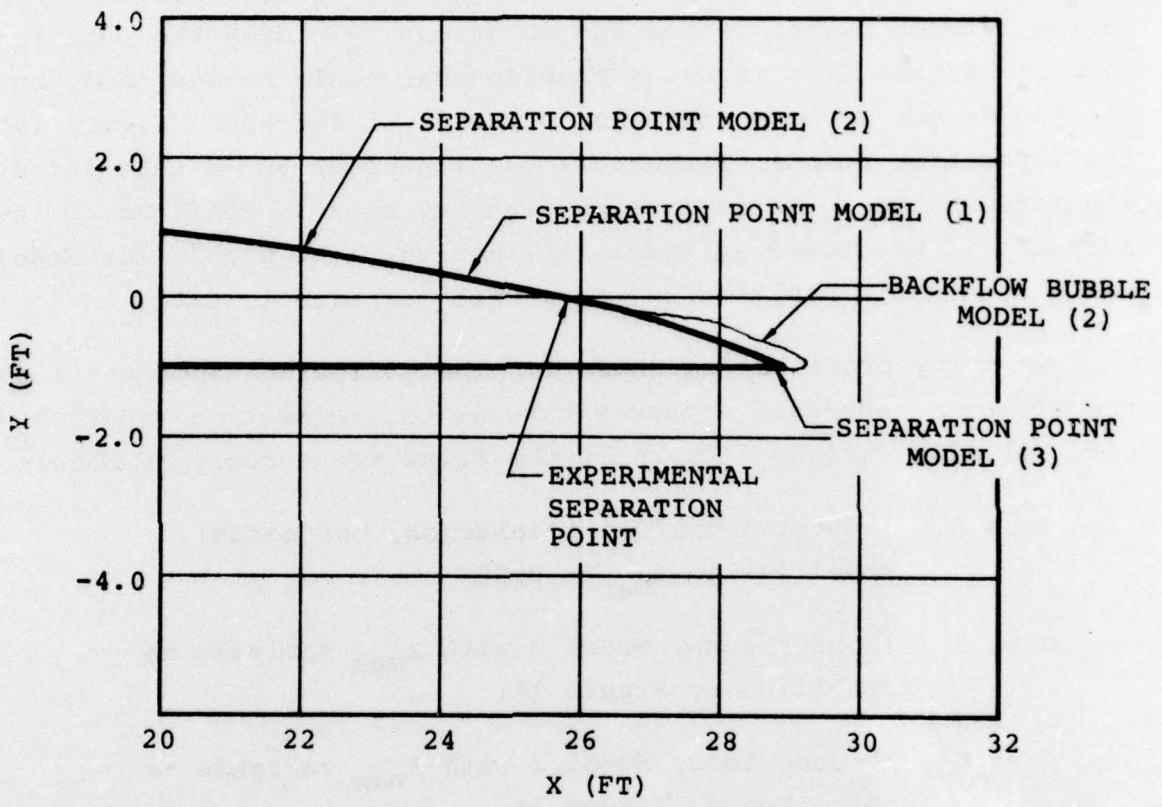

Figure 19. Experimental and Calculated Separation Points.

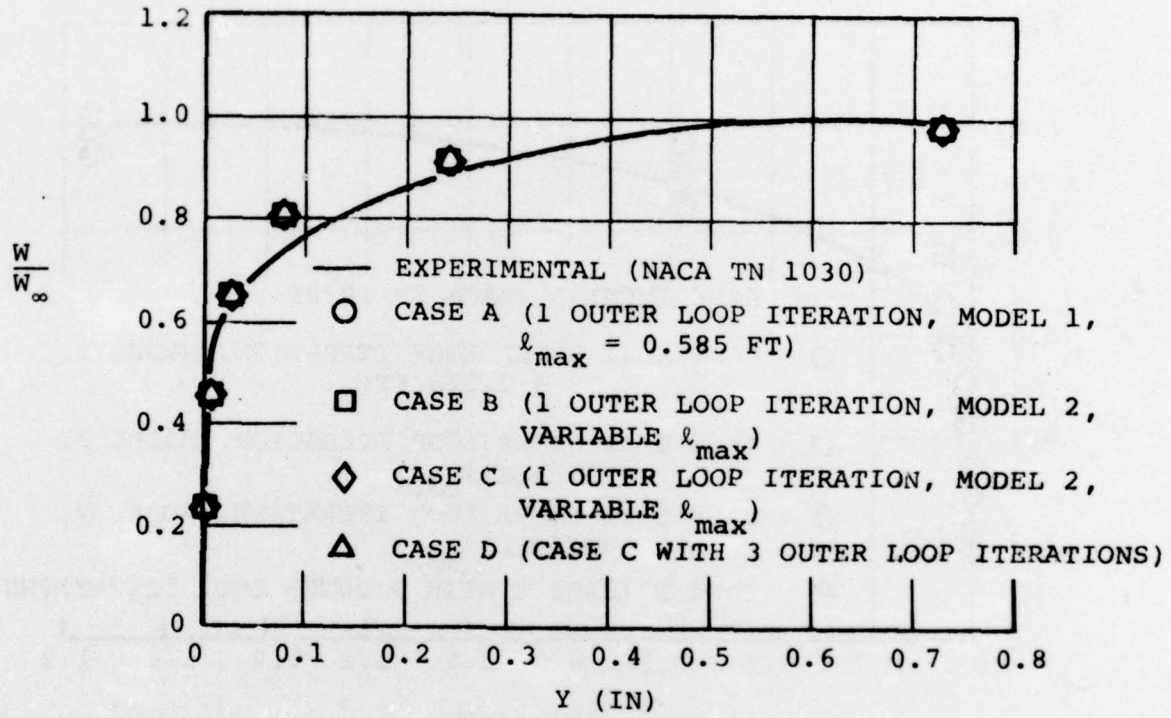

Figure 20. Comparisons of Calculations to Experimental Boundary Layer Velocity Profile at X = 3.5 Ft.

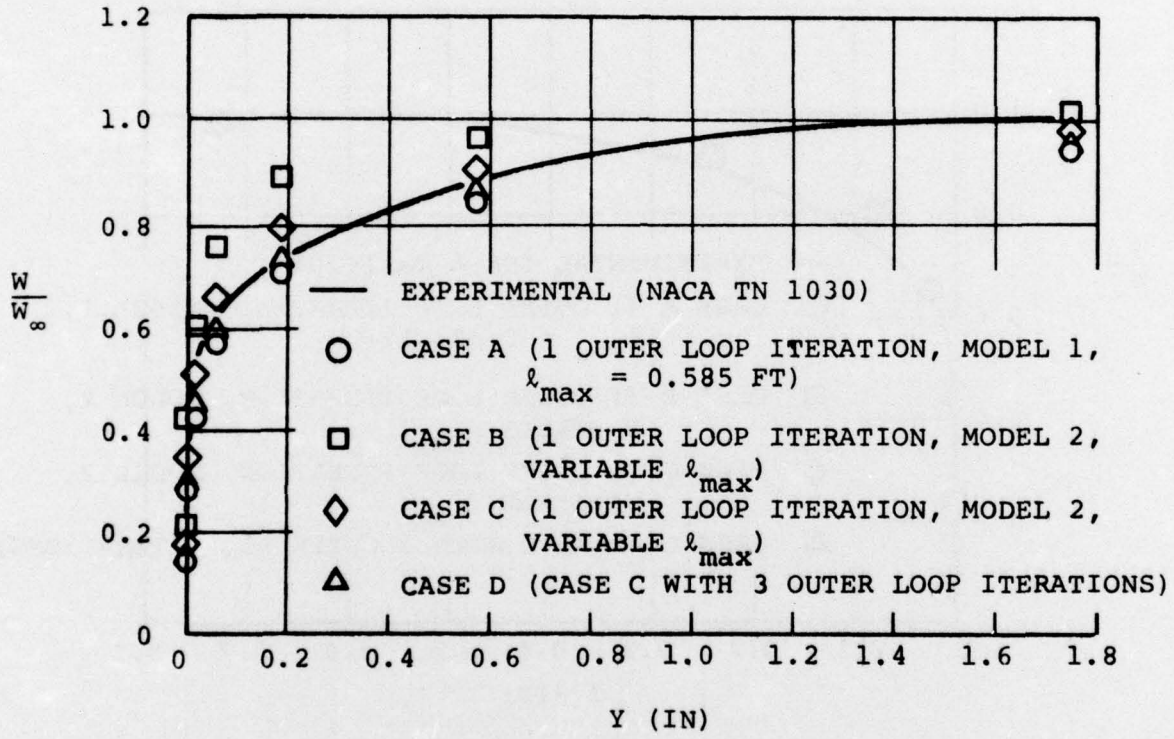

Figure 21. Comparisons of Calculations to Experimental Boundary Layer Velocity Profile at X = 10.5 Ft.

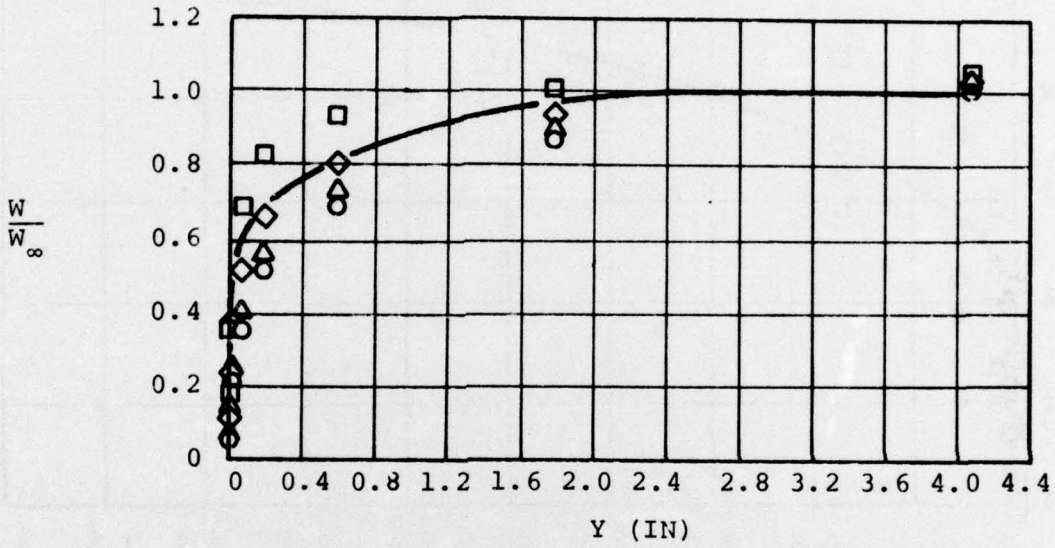

—— EXPERIMENTAL (NACA TN 1030)

○ CASE A (1 OUTER LOOP ITERATION, MODEL 1, ℓ_{max} = 0.585 FT)

□ CASE B (1 OUTER LOOP ITERATION, MODEL 2, VARIABLE ℓ_{max})

◇ CASE C (1 OUTER LOOP ITERATION, MODEL 2 VARIABLE ℓ_{max})

△ CASE D (CASE C WITH 3 OUTER LOOP ITERATIONS)

Figure 22. Comparisons of Calculations to Experimental Boundary Layer Velocity Profile at X = 17.5 Ft.

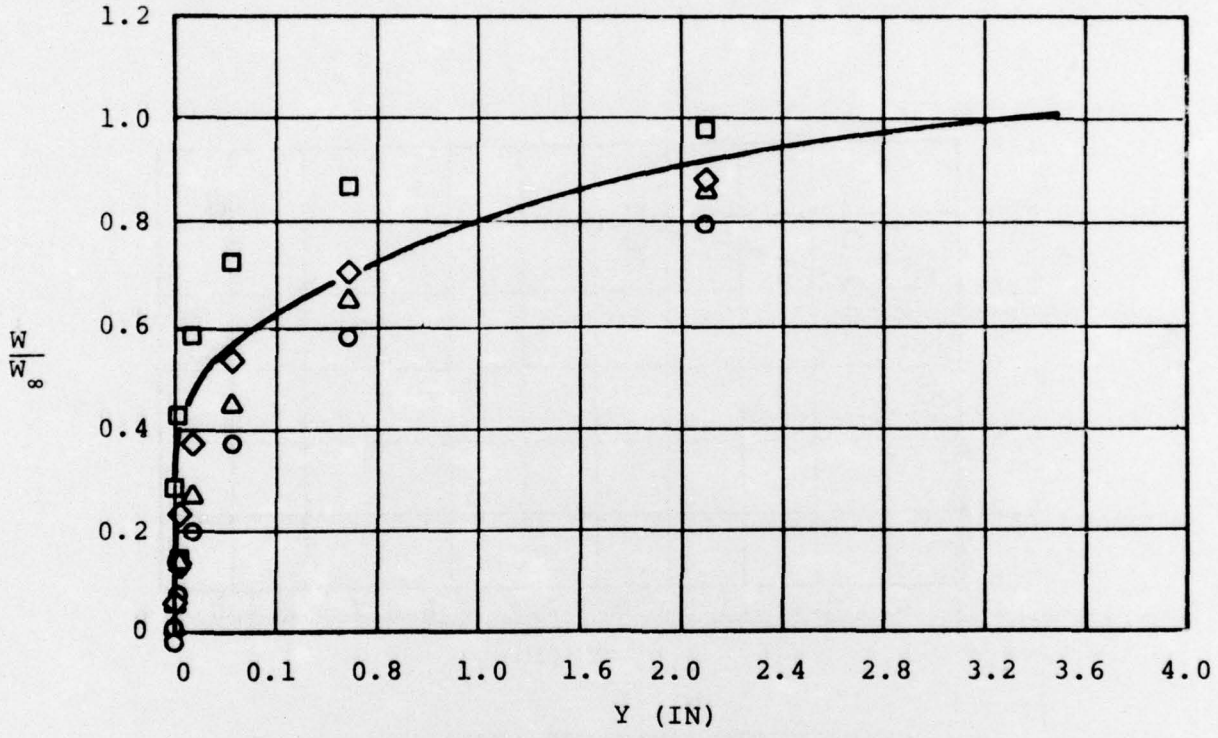

—— EXPERIMENTAL (NACA TN 1030)

○ CASE A (1 OUTER LOOP ITERATION, MODEL 1, ℓ_{max} = 0.585 FT)

□ CASE B (1 OUTER LOOP ITERATION, MODEL 2, VARIABLE ℓ_{max})

◇ CASE C (1 OUTER LOOP ITERATION, MODEL 2 VARIABLE ℓ_{max})

△ CASE D (CASE C WITH 3 OUTER LOOP ITERATIONS)

Figure 23. Comparisons of Calculations to Experimental Boundary Layer Velocity Profile at X = 21.0 Ft.

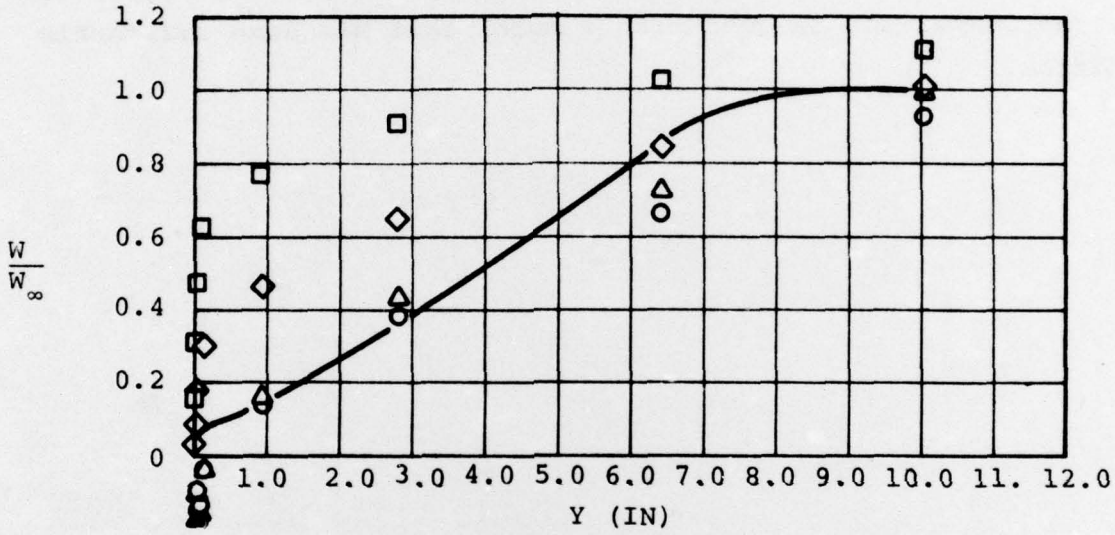

——— EXPERIMENTAL (NACA TN 1030)

○ CASE A (1 OUTER LOOP ITERATION, MODEL 1, ℓ_{max} = 0.585 FT)

□ CASE B (1 OUTER LOOP ITERATION, MODEL 2, VARIABLE ℓ_{max})

◇ CASE C (1 OUTER LOOP ITERATION, MODEL 2, VARIABLE ℓ_{max})

△ CASE D (CASE C WITH 3 OUTER LOOP ITERATIONS)

Figure 24. Comparisons of Calculations to Experimental Boundary Layer Velocity Profile at X = 25.77 Ft.

The results of these calculations were not intended to provide a turbulence model of any great universality, but rather to demonstrate the viability of this technique for solution of the fluid dynamic equations. Indeed, the effect of turbulence complicates the evaluation since the base accuracy of the method cannot be assessed. Nevertheless, the comparison is good with a model that has some reasonable foundation.

7.0 CONCLUSIONS

The above sections have outlined a method that offers the potential for rapid solutions to the Navier-Stokes equations. Run times for the problem described in Section 6.0 were less than 7 minutes on a CDC 6400. Substantial improvement to this could easily have been made by improving the coding efficiency in both the relaxation and marching sections. The solution method reduces the expensive relaxation portion of the calculation to just that needed to compute static pressure.

The ~~viscous~~ Navier-Stokes equation is solved by a single-pass marching process, which overcomes the mathematical difficulties imposed, by transforming the solution in the direction normal to the flow into a spectral plane. The method has been verified, as far as possible. However, a precise determination of accuracy is clouded by the uncertainties introduced by turbulence and the modeling thereof. Nevertheless, it has been shown that the method yields reasonable results both in a full solution to the flow around a shaped body, and in a variety of plate flows with and without pressure gradients. Further exercise of the method would be greatly enhanced by the inclusion of compressibility effects, which would allow study of shock boundary layer interactions where significant laminar data exists.